

# Contact State Estimation for Legged Robots

*Michael Maravgakis*

Thesis submitted in partial fulfillment of the requirements for the  
*Masters' of Science degree in Computer Science and Engineering*

University of Crete  
School of Sciences and Engineering  
Computer Science Department  
Voutes University Campus, 700 13 Heraklion, Crete, Greece

Thesis Advisor: Prof. *Panos Trahanias*

---

This work has been performed at the University of Crete, School of Sciences and Engineering, Computer Science Department.

The work has been supported by the Foundation for Research and Technology - Hellas (FORTH), Institute of Computer Science (ICS).



UNIVERSITY OF CRETE  
COMPUTER SCIENCE DEPARTMENT

**Contact State Estimation for Legged Robots**

Thesis submitted by  
**Michael Maravgakis**  
in partial fulfillment of the requirements for the  
Masters' of Science degree in Computer Science

THESIS APPROVAL

Author: \_\_\_\_\_  
Michael Maravgakis

Committee approvals: \_\_\_\_\_  
Panos Trahanias  
Professor, Thesis Supervisor

\_\_\_\_\_  
Antonios Argyros  
Professor, Committee Member

\_\_\_\_\_  
Dimitrios Papageorgiou  
Assistant Professor, Committee Member

Departmental approval: \_\_\_\_\_  
Polyvios Pratikakis  
Associate Professor, Director of Graduate Studies

Heraklion, June 2023



# Contact State Estimation for Legged Robots

## Abstract

Legged robot locomotion in unstructured and slippery terrains relies heavily on accurately identifying the contact state between the robot’s feet and the ground. Contact state estimation poses significant challenges, typically addressed by leveraging force measurements, joint encoders as well as robot kinematics and dynamics. This thesis introduces two novel approaches for accurately estimating the contact state in real-time, namely, a deep learning approach and a probabilistic model-based method.

To address the challenges of leg contact detection in bipedal walking gaits, a deep learning framework is proposed. This framework accurately and robustly estimates the contact state probability for each leg, distinguishing between stable contact, slip, or no contact. Notably, the framework relies solely on proprioceptive sensing and demonstrates generalizability across diverse friction surfaces and legged robotic platforms. Comprehensive evaluations, including comparisons with state-of-the-art methods, have been performed using ATLAS, NAO, and TALOS humanoid robots. Furthermore, the framework’s efficacy is demonstrated in real-world base estimation tasks with a TALOS humanoid robot.

The second proposed approach is model-based and relies solely on Inertial Measurement Units (IMUs) mounted on the robot’s end effectors. It offers a versatile approach that can be implemented in any legged robot without the necessity of training data. By capitalizing on the uncertainty of IMU measurements, this novel probabilistic method is capable of estimating the probability of stable contact. The method approximates the multimodal probability density function using Kernel Density Estimation, providing reliable contact state estimation. Extensive evaluations of the proposed method have been conducted on both real and simulated scenarios, demonstrating its effectiveness on various bipedal and quadrupedal robotic platforms, including ATLAS, TALOS, and Unitree’s GO1.

Finally, this thesis introduces an application of the aforementioned probabilistic contact state estimator that further demonstrates its efficacy. More specifically, an adaptive trajectory tracking controller is presented, which was developed by peers in the Computational Vision and Robotics Laboratory. This controller consists of two prioritized layers of adaptation aimed at preventing leg slippage when stepping on partially or globally slippery terrains. The primary emphasis is placed on the results, as the first layer of adaptation effectively utilizes the contact probability to distribute the effort among each leg. Therefore, the accuracy of this controller is directly correlated to the ability to estimate the contact state in real-time which validates the robustness of the proposed contact estimator.



# Εκτίμηση Κατάστασης Επαφής σε Βαδίζοντα Ρομπότ

## Περίληψη

Η κίνηση των βαδίζοντων ρομπότ σε ανώμαλα και ολισθηρά εδάφη εξαρτάται σε μεγάλο βαθμό από την ακριβή αναγνώριση της κατάστασης επαφής μεταξύ των ποδιών του ρομπότ και του εδάφους. Ο τομέας της εκτίμησης της κατάστασης επαφής αντιμετωπίζει σημαντικές προκλήσεις, οι οποίες προσεγγίζονται συνήθως μέσω της εκμετάλλευσης μετρήσεων δυνάμεων, κωδικοποιητών αρθρώσεων καθώς και της κινηματικής και δυναμικής του ρομπότ. Στην παρούσα διατριβή παρουσιάζονται δύο νέες προσεγγίσεις για την ακριβή εκτίμηση της κατάστασης επαφής σε πραγματικό χρόνο: ένα μοντέλο βαθιάς μάθησης και ένα πιθανοτικό μοντέλο.

Για την αντιμετώπιση των προκλήσεων της ανίχνευσης επαφής ποδιού κατά τη βάδιση δίποδων ρομποτ, προτείνεται κατάρχην μία αρχιτεκτονική βαθιάς μάθησης. Η αρχιτεκτονική αυτή εκτιμά με ακρίβεια και αξιοπιστία την κατάσταση επαφής για κάθε πόδι, διακρίνοντας μεταξύ σταθερής επαφής, ολίσθησης ή μη επαφής. Σημαντικό είναι ότι το πλαίσιο αυτό βασίζεται αποκλειστικά στην αισθητηριακή αντίληψη του ρομπότ και επιδέχεται γενίκευση σε ποικίλες επιφάνειες τριβής αλλά και ρομποτικών πλατφόρμων. Πραγματοποιήθηκαν εκτενείς αξιολογήσεις, συμπεριλαμβανομένων συγκρίσεων με προηγμένες μεθόδους, χρησιμοποιώντας ανθρωποειδή ρομπότ, όπως τα ATLAS, NAO και TALOS. Επιπλέον, η αποτελεσματικότητα της προτεινόμενης μεθόδου αποδεικνύεται σε πραγματικές συνθήκες εκτίμησης κατάστασης με ένα δίποδο TALOS.

Η δεύτερη προτεινόμενη προσέγγιση μοντελοποιεί τα χαρακτηριστικά της επαφής και βασίζεται αποκλειστικά σε μονάδες μέτρησης αδράνειας (IMUs) που τοποθετούνται στα άκρα του ρομπότ. Η μέθοδος αυτή προσφέρει μια ευέλικτη προσέγγιση που μπορεί να εφαρμοστεί σε οποιοδήποτε βαδίζον ρομπότ χωρίς να απαιτούνται δεδομένα για εκπαίδευση. Αξιοποιώντας την αβεβαιότητα των μετρήσεων αδράνειας, παρουσιάζεται ένας νέος πιθανοτικός τρόπος για την εκτίμηση της πιθανότητας σταθερής επαφής. Η μέθοδος προσεγγίζει την πολυμεταβλητή πυκνότητα πιθανότητας χρησιμοποιώντας την μέθοδο Kernel Density Estimation, παρέχοντας αξιόπιστη εκτίμηση της κατάστασης επαφής. Έχουν πραγματοποιηθεί εκτενείς αξιολογήσεις της προτεινόμενης μεθόδου σε πραγματικά και προσομοιωμένα σενάρια, αποδεικνύοντας την αποτελεσματικότητά της σε διάφορες ρομποτικές πλατφόρμες, συμπεριλαμβανομένων των ATLAS, TALOS και GO1 της Unitree.

Τέλος, αυτή η διατριβή παρουσιάζει μια εφαρμογή του προαναφερθέντος πιθανοτικού εκτιμητή κατάστασης επαφής που επιδεικνύει περαιτέρω την αποτελεσματικότητά του. Συγκεκριμένα, παρουσιάζεται η εφαρμογή σε ένα προσαρμοσμένο ελεγκτή τροχιάς που αναπτύχθηκε από συναδέλφους στο Εργαστήριο Υπολογιστικής Όρασης και Ρομποτικής. Αυτός ο ελεγκτής αποτελείται από δύο επίπεδα προσαρμογής με στόχο την αποφυγή ολίσθησης των ποδιών σε μερικώς ή ολικώς ολισθηρές επιφάνειες. Κυρίως, δίνεται έμφαση στα αποτελέσματα, καθώς το πρώτο επίπεδο

προσαρμογής χρησιμοποιεί την πιθανότητα επαφής για την κατανομή της προσπάθειας σε κάθε πόδι. Επομένως, η ακρίβεια αυτού του ελεγκτή σχετίζεται άμεσα με την ικανότητα εκτίμησης της κατάστασης επαφής σε πραγματικό χρόνο, καθιστώντας έτσι τον προτεινόμενο εκτιμητή επαφής αξιόπιστο.

## Acknowledgements

I would like to express my deepest gratitude and appreciation to Prof. Panos Trahanias for his exceptional guidance, constant support, and inspiration throughout my journey in completing this MSc thesis. I am truly fortunate to have had the opportunity to work under his supervision. I am also indebted to the members of Computational Vision and Robotics Laboratory (CVRL) at ICS-FORTH for our fruitful discussions and encouragement, and for providing me with a stimulating and collaborative research environment.

I extend my heartfelt thanks to the members of the MSc committee, Prof. Antonis Argyros and Assistant Prof. Dimitrios Papageorgiou, for their valuable comments and suggestions. Their input and constructive feedback have significantly contributed to the refinement and improvement of my research.

I am deeply indebted to Dr. Stylianos Piperakis for his invaluable guidance, expert advice, and continuous support throughout this challenging journey. His insightful comments and thoughtful suggestions have immensely shaped the direction of my research. I am grateful for his unwavering belief in my abilities and his dedication to help me overcome obstacles along the way.

I would like to express my sincere appreciation to the Foundation for Research and Technology-Hellas (FORTH) and the University of Crete for providing financial support and laboratory equipment, which has enabled me to pursue this MSc degree and conduct my research. The academic environment provided by these esteemed institutions has been instrumental in fostering my intellectual growth and development.

Finally, I would like to express my deepest gratitude to my family, friends, and Vicky for their unwavering support during both the highs and lows of this journey. Their encouragement and understanding have provided me with the strength and motivation to persevere.



# Contents

<b>Table of Contents</b>	<b>i</b>
<b>List of Figures</b>	<b>iii</b>
<b>List of Tables</b>	<b>v</b>
<b>1 Introduction</b>	<b>1</b>
1.1 Legged Robots Landscape . . . . .	1
1.1.1 Challenges . . . . .	3
1.1.2 Legged Locomotion Scheme . . . . .	4
1.2 Thesis Motivation . . . . .	5
1.3 Thesis Scope and Contribution . . . . .	6
1.3.1 Contributed Papers . . . . .	6
1.3.2 Open-source Software . . . . .	7
1.4 Thesis outline . . . . .	7
<b>2 Related Work</b>	<b>9</b>
2.1 Simple Threshold . . . . .	9
2.2 Schmidt-Trigger . . . . .	10
2.3 State-of-the-art . . . . .	11
2.3.1 Model-based approaches . . . . .	11
2.3.2 Learning-based approaches . . . . .	12
<b>3 Significance of Contact State Estimation</b>	<b>15</b>
3.1 Base State Estimation . . . . .	15
3.2 Bipedal Locomotion & CoM Estimation . . . . .	17
<b>4 Robust Contact State Estimation in Humanoid Walking Gaits</b>	<b>21</b>
4.1 Training Data Acquisition . . . . .	22
4.1.1 Contact State in the Centroidal Dynamics . . . . .	22
4.1.2 Contact State in the Leg Kinematics . . . . .	23
4.2 Robust Contact Estimation with Deep Learning . . . . .	23
4.2.1 Preprocessing . . . . .	24
4.2.2 Architecture . . . . .	25

4.3	Results . . . . .	25
4.3.1	Simulation Results . . . . .	25
4.3.2	Comparison to Thresholding methods . . . . .	27
4.3.3	Comparison to unsupervised learning . . . . .	29
4.3.4	LCD with feature reduction . . . . .	30
4.3.5	Experimental Results: Application to Base Estimation . . . . .	30
4.3.6	Discussion . . . . .	30
4.4	Conclusions . . . . .	31
<b>5</b>	<b>Probabilistic Contact State Estimation for Legged Robots using Inertial Information</b>	<b>33</b>
5.1	Problem Formulation . . . . .	34
5.1.1	Background . . . . .	34
5.1.2	Measurement Model . . . . .	35
5.1.3	Complementary Filter . . . . .	36
5.1.4	Stable contact definition . . . . .	37
5.2	Mathematical Modeling . . . . .	37
5.3	Results . . . . .	39
5.3.1	Simulation Results . . . . .	40
5.3.2	Real experiments . . . . .	41
5.3.3	Comparative evaluation . . . . .	43
5.4	Conclusions . . . . .	45
<b>6</b>	<b>Two-layer adaptive trajectory tracking controller for quadruped robots on slippery terrains</b>	<b>47</b>
6.1	Problem Formulation . . . . .	47
6.2	Proposed Scheme . . . . .	49
6.2.1	First layer of adaptation: Adaptive effort distribution . . . . .	49
6.2.2	Second layer of adaptation: Trajectory time-scaling . . . . .	49
6.3	Simulation study . . . . .	51
6.3.1	Scenario 1: Point to point motion . . . . .	51
6.3.2	Scenario 2: One-foot slippage . . . . .	52
6.3.3	Scenario 3: Global slippage . . . . .	54
6.4	Experimental validation . . . . .	55
6.5	Conclusions . . . . .	57
<b>7</b>	<b>Conclusions</b>	<b>59</b>
7.1	Summary . . . . .	59
7.2	Future Work . . . . .	60
	<b>Bibliography</b>	<b>63</b>

# List of Figures

1.1	State-of-the-art legged robots . . . . .	2
1.2	Legged Locomotion Scheme . . . . .	4
1.3	Visualization of robot’s perception and step planner for Atlas humanoid robot [1]. . . . .	5
2.1	Smoothed vertical ground reaction force of Atlas’ left foot for five steps with <b>simple threshold</b> . . . . .	10
2.2	Smoothed vertical ground reaction force of Atlas’ left foot for five steps with <b>Schmidt-Trigger</b> . . . . .	11
3.1	Simulated GO1 quadruped robot with base, foot and world frames	16
3.2	Humanoid robot walking [2] . . . . .	18
4.1	LCD Deep Learning Architecture. . . . .	24
4.3	Thresholding and LCD predictions for SC on ATLAS walking gaits with varying friction coefficient surfaces . . . . .	28
4.4	Unsupervised learning and LCD predictions on normal and low friction gaits. . . . .	29
4.5	3D-Base position error of the estimated base position with SEROW from the corresponding ground-truth base position. . . . .	31
5.1	Static and Kinetic friction force. . . . .	34
5.2	Force fluctuations during impact for the ATLAS simulated robot. .	36
5.3	Example of estimated PDF for 100 $a_x$ samples. . . . .	39
5.4	ATLAS walking on stable surface. . . . .	40
5.5	Estimated stable contact probabilities for ATLAS gaits on slippery terrain. . . . .	41
5.6	TALOS walking on a stable surface. . . . .	42
5.7	GO1 walking on soft terrain/low restitution. . . . .	42
5.8	GO1 walking on slippery terrain for 3 consecutive steps. . . . .	43
5.9	Comparative results; top row: vertical GRF; middle row: Contact probabilities as computed by proposed method; bottom row: Contact probabilities as computed by [3]. . . . .	44
5.10	Histograms of the difference between predicted contact probability and ground truth labels. . . . .	44

6.1	Force distribution among the legs of the quadruped robot. . . . .	48
6.2	Convergence of the control effort of each leg towards the friction cone. . . . .	50
6.3	The initial configuration of the simulations. Yellow area: The slippery area considered for the second scenario. . . . .	51
6.4	[Scenario 1: Point-to-point motion] Time evolution of the actual and desired position. . . . .	52
6.5	[Scenario 2: One-foot slippage] Weight adaptation due to the first layer (the second layer is not enabled). . . . .	53
6.6	[Scenario 2: One-foot slippage] Position and orientation error norms with and without adaptation. . . . .	53
6.7	[Scenario 3: Global slippage] Weight adaptation due to the first and second layer. . . . .	54
6.8	[Scenario 3: Global slippage] Evolution of the position of the CoM in time, with and without adaptation. . . . .	55
6.9	The experimental setup and initial configuration of the robot. . . . .	55
6.10	The second weight during the experimental validation. . . . .	56
6.11	Evolution of the position of the CoM in time, with and without adaptation. . . . .	57

# List of Tables

4.1	Simulation noise standard deviations. . . . .	27
4.2	LCD evaluation on variable friction datasets . . . . .	28
4.3	LCD performance with reduced features . . . . .	30



# Chapter 1

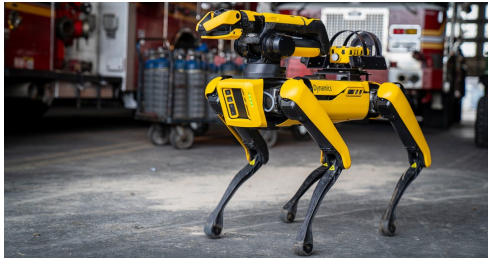
## Introduction

The field of robotics has experienced significant progress in recent years, revolutionizing industries from manufacturing and surveillance to transportation and agriculture. As robots become more advanced, they are able to perform tasks that were previously deemed impossible or too dangerous for humans to undertake. Furthermore, the integration of artificial intelligence and machine learning in robotics has enabled them to adapt and learn autonomously, increasing their efficiency and usefulness, while at the same time fostering human-robot interaction. In the future, the field of robotics is expected to continue making significant contributions towards improving productivity, enhancing safety, and solving complex problems in various fields.

### 1.1 Legged Robots Landscape

Legged robots in particular, are becoming increasingly important in various fields such as search and rescue, exploration and logistics operations. Unlike wheeled and flying robots, legged robots have the ability to discretize space which enables them to traverse rough terrains and navigate through unstructured and dynamic environments, for instance sewers or construction sites. The dynamic human-centric environment, that is imperative for robots to navigate into, constitutes their deployment in real-world scenarios generally challenging. Environments such as multi-level buildings or construction sites consist of discontinuous terrains, such as stairs and obstacles. The morphology of legged robots is by design appropriate of such terrains, enabling them to strategically plan and execute discrete footholds in order to traverse them.

In recent years, significant advancements have been made in legged robot technology, particularly in hardware and sensory equipment, which have led to the development of increasingly capable and robust robotic platforms (Fig. 1.1). Modern legged robots are also equipped with numerous sensors for reliable perception of the environment such as depth and stereo camera systems, Light Detection And Ranging (LiDAR) and ultrasonic sensors. Moreover, within the realm of hardware,



(a) Spot: Quadrupedal robot by Boston Dynamics<sup>1</sup>



(b) Digit: Bipedal robot by Agility Robotics<sup>2</sup>

Figure 1.1: State-of-the-art legged robots

notable progress has also been made in actuation and battery autonomy, while feedback sensory has evolved into a more sophisticated technology with faster and more accurate proprioceptive sensors, namely, Inertial Measurement Units (IMU), force/torque sensors (F/T) and joint encoders. These sensors provide essential information for dynamic legged locomotion and state estimation.

Nowadays, and despite the increasing interest in legged robots, only a limited number of companies are engaged in the development of multi-legged robots, and even fewer specialize in the design and commercialization of bipedal robots. The latter offers several advantages over other  $k$ -legged robots ( $k > 2$ ). In comparison, humanoids exhibit greater ability to interact with their environment and manipulate objects, due to their anthropomorphic design. The world we live in is designed by humans for humans, making humanoid robots' morphology optimal for navigation, interaction and manipulation of their surroundings. Moreover, the similarity with humans facilitates better human-robot interaction, enabling their seamless cooperation. Additionally, humanoid robots can take advantage of human tools and devices, which constitutes them even more versatile and useful in various applications. These advantages make humanoid robots a desirable option in various fields, including healthcare, logistics and manufacturing, by helping humans optimize their workflow and avoid performing labor intensive repetitive tasks. Nevertheless, the domains of legged locomotion and state estimation are becoming profoundly competitive, being actively pursued by a limited number of research groups worldwide. Despite the fact that legged robots are considered as one of the most promising robotic platforms for collaborating and cooperating with humans in a work environment, there are still several challenges that need to be addressed.

<sup>1</sup><https://www.bostondynamics.com/products/spot>

<sup>2</sup><https://agilityrobotics.com/robots>

### 1.1.1 Challenges

As stated previously, the main advantage of legged robots over other mobile robots is the ability to traverse an environment by planning and executing discrete foot-steps, thus enabling their navigation in unstructured and cluttered terrains. Consequently, this characteristic inherently introduces instability to the robot, which requires to be addressed by employing complex and interdisciplinary approaches. The main challenges and open research problems in the field of legged robotics are outlined below:

- **Gait Planning and Control:** Legged robots require complex and adaptive control strategies to achieve stable and efficient motion. Designing effective gait patterns that can be executed in real-time and adapting them to various environmental conditions is a significant challenge [4]. Contemporary approaches [5, 6, 7] explore reinforcement learning for tackling this challenge and demonstrating resilient gaiting behavior and stability.
- **State Estimation:** It is the process of estimating the robot's current state, which includes its position, orientation, velocity, **contact state** and other relevant variables. This is typically accomplished by fusing both proprioceptive and exteroceptive sensory information as well as previous estimates. For legged robots, state estimation can be challenging due to the complex dynamics and the multiple contact points between the robot's feet and the ground [8, 9, 10]. The robot's state can change rapidly and unpredictably as it moves, and it must be estimated in real-time for the robot to maintain stability and perform complex tasks. Most commonly, state estimation approaches utilize various sensors, such as IMUs, encoders, and other proprioceptive sensors. However, these sensors tend to be noisy and prone to errors, which can lead to inaccurate state estimates and eventually instability.
- **Sensing and Perception:** Legged robots require accurate, fast and reliable sensing in order to navigate through complex and dynamic environments [11, 12, 13]. They must possess the ability to perceive and respond to obstacles and sudden changes in their surroundings, which can be challenging in outdoor or unstructured environments. The main drawback is that exteroceptive sensors (cameras, LiDARs etc.) usually operate in low refresh rates which constrains the response time of the robot when an obstacle is detected. Moreover, such sensors are greatly affected by the structure of the surrounding environment (glass doors/windows, poor light conditions etc.).
- **Simultaneous Localization and Mapping (SLAM):** Mobile robots, in general, usually rely on SLAM in order to navigate autonomously in complex environments. In the case of legged robots, every link of the robot is both translating and rotating with respect to a world frame/map origin during locomotion. The changing pose of the sensor (which needs to be attached at a link) makes it challenging to perform SLAM, adding significant complexity

to the process. To address this problem, it is necessary to consider the current state of the robot, the gait phase [14], impact oscillations resulting from large Ground Reaction Forces (GRFs), and the robot’s **quality of contact** with ground.

### 1.1.2 Legged Locomotion Scheme

Legged locomotion is an interdisciplinary field that requires fast sensors, real-time computations and data processing. The outline of the pipeline for achieving dynamic legged locomotion is graphically illustrated in Fig. 1.2. The main nodes from this graph, which depend on each other, are the *Motion Planner*, *Feedback Controller* and *State Estimation*, while the generic *Dynamic System* represents the robot.

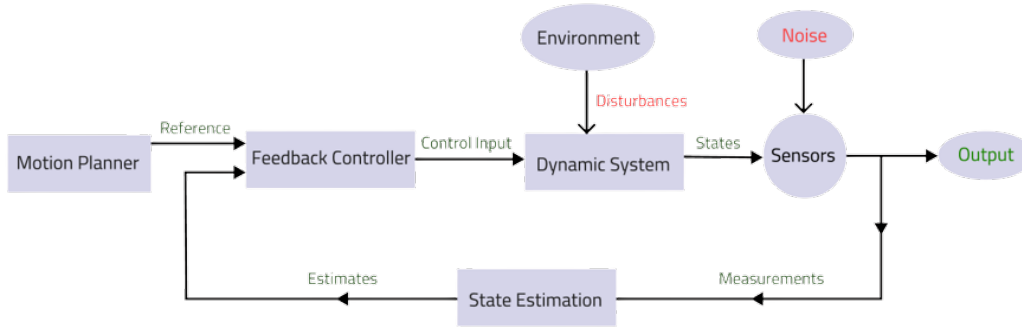


Figure 1.2: Legged Locomotion Scheme

The *Motion Planner* is responsible for generating a reference trajectory that the robot needs to follow in order to achieve the goal. In legged robotics, the motion planner contains many layers and one of them is the step planner. The step planner’s purpose is to generate six-dimensional goal poses in space that represent desired position and orientation of each foothold. In Fig. 1.3, a visualization of multiple planned steps is provided for the Atlas humanoid robot, alongside with a sparse heatmap that illustrates how the robot perceives its surroundings.

The *Feedback Controller* is responsible for communicating with the actuators and by taking into account the current state, produce the desired motion. There are many feedback controller designs for ensuring that the robot will perform the commanded action. Some widely used model-based techniques are Proportional Integral Derivative (PID), Model Predictive Control (MPC) and linear quadratic regulator. Contemporary research endeavours introduced the deployment of machine learning for extracting the dynamics of the system and automatically tune the controller, for instance reinforcement learning and fuzzy control.

Finally, *State Estimation* techniques provide the necessary feedback to the controller by estimating vital variables in real-time. It does so by fusing erroneous sensor measurements into more accurate estimates while considering the previous

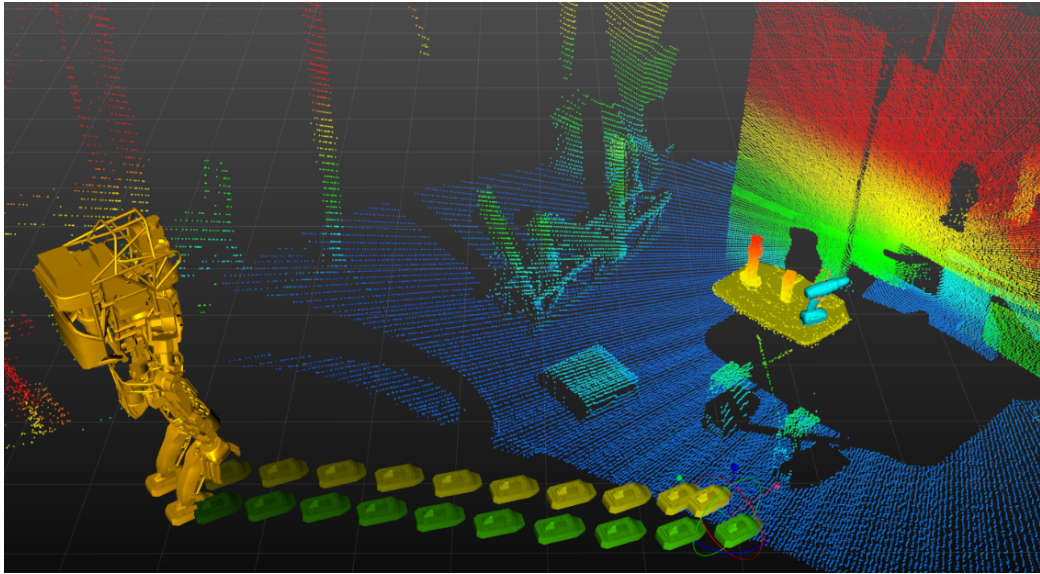


Figure 1.3: Visualization of robot’s perception and step planner for Atlas humanoid robot [1].

state of the system. The state of the robot is of arbitrary dimension while the bare minimum includes the pose of the base frame or in some cases, a frame attached to the Center of Mass (CoM). Information regarding the exact position of the CoM is generally unobtainable due to the heterogeneity of the mass distribution in the torso (e.g. battery located to one side and computer board to the other). On the contrary, the base frame is an arbitrary frame that is attached somewhere in the robot’s torso. Although its pose is user-defined, it is most of the times attached to a suitable place in order to facilitate the relative transformations between the base and every other link and joint. Other useful state variables that usually need to be estimated is the position of the CoM paired with the forces acting on it, the gait phase and the **contact state**.

## 1.2 Thesis Motivation

Legged robots rely solely on discrete contacts between their feet and the ground to interact with the environment and induce motion to their base, thereby, accurately generating the required forces on the CoM is essential in attaining functional locomotion. The main challenges that the field of legged robotics is currently facing were concisely described in section 1.1.1. Most of these challenges/research areas directly depend on accurate and real-time knowledge of the contact state. For instance, the lack of knowledge regarding whether the foot has slipped in the preceding step can induce catastrophic consequences since the motion planner will produce a trajectory based on false foot pose. As a consequence, the controller

might try to perform an action that is restricted either by the environment (e.g. collision with the ground) or its mechanical constraints. Finally, in the event of slippage, the robot will experience significant drift in odometry, ultimately resulting in the loss of position tracking. An extensive analysis regarding the necessity of accurate contact state estimation is presented in Chapter 3.

### 1.3 Thesis Scope and Contribution

The objective of this thesis is to explore the issue of contact state estimation for bipedal and quadruped robots and suggest proper methods to cope with that. While determining the contact state is crucial for the development of locomotion and state estimation algorithms, its significance extends beyond these applications.

The main contributions of this thesis are two novel approaches for estimating the contact state in quadruped and bipedal robots. The first approach utilizes machine learning to classify the contact state on bipedal robots while the second one introduces a probabilistic method for extracting the quality of contact (probability the contact is stable) of  $k$ -legged robots. Both proposed approaches rely solely on proprioceptive sensing and operate in real-time. Moreover, the proposed approaches were extensively tested and compared against other approaches in both real and simulated legged robots. Finally, an adaptive controller developed by peers in the Computational Vision and Robotics Laboratory, utilized the probabilistic approach as the basis of the adaptive control law for the joint weights. The specific contributions to the state-of-the-art of each method will be stated explicitly in the respective chapters.

#### 1.3.1 Contributed Papers

Most parts of this thesis have been published and presented in high-impact conferences in the relevant scientific field:

- **Michael Maravgakis**, Despina-Ekaterini Argiropoulos, Stylianos Piperakis and Panos Trahanias, "Probabilistic Contact State Estimation for Legged Robots using Inertial Information", *2023 International Conference on Robotics and Automation (ICRA), London, England*. [15]
- Stylianos Piperakis, **Michael Maravgakis**, Dimitrios Kanoulas, and Panos Trahanias, "Robust Contact State Estimation in Humanoid Walking Gaits", *2022 IEEE/RSJ International Conference on Intelligent Robots and Systems (IROS), Kyoto, Japan*. [16]
- Despina-Ekaterini Argiropoulos, Dimitrios Papageorgiou, **Michael Maravgakis**, Drosakis Drosakis and Panos Trahanias, "Two-layer adaptive trajectory tracking controller for quadruped robots on slippery terrains" (under preparations to be submitted at ICRA 2024).

### 1.3.2 Open-source Software

To reinforce further research endeavors, both proposed approaches and the adaptive controller are offered as open-source projects to the community by visiting the following public repositories:

- ROS/Python: Legged Contact Detection (LCD)  
*Author:* Michael Maravgakis  
<https://github.com/michaelMarav/lcd>
- ROS/Python: Probabilistic Contact Estimation (PCE)  
*Author:* Michael Maravgakis  
<https://github.com/MichaelMarav/ProbabilisticContactEstimation>
- ROS/C++: Two-Layer Adaptive Controller (Maestro)  
*Author:* Despina-Ekaterini Argiropoulos  
<https://github.com/despargy/maestro/>

## 1.4 Thesis outline

This thesis is organized as follows:

- Chapter 2 presents the contemporary related work in the field of contact state estimation while also explicates the most widely used heuristic approaches in the field.
- Chapter 3 provides a qualitative and analytical exploration of the significance of contact estimation within the domain of base state estimation, bipedal locomotion, and CoM estimation.
- Chapter 4 proposes a supervised deep learning framework for estimating the contact state in bipedal robots.
- Chapter 5 introduces a model-based probabilistic approach for extracting the stable contact probability in legged robots.
- Chapter 6 briefly presents an adaptive controller that utilizes the proposed model-based approach to suitably adapt the joint weights for trajectory planning. This chapter mainly emphasizes on the results which are directly correlated with the robustness of the proposed contact state estimator.
- Chapter 7 concludes this thesis outlining the main contributions to the relevant research field and discusses possible future research objectives.



## Chapter 2

# Related Work

To achieve truly agile and dexterous locomotion, possessing the ability to accurately estimate the contact state in real-time is indispensable. To this end, accurate and robust foot contact detection entails a vital role in locomotion control [17, 18, 19], gait planning [20, 21, 22], base state estimation [23, 24, 25, 26] and Center of Mass (CoM) estimation [27, 28, 29]. However, this topic remains largely unexplored and many approaches assume that the contact will be stable a priori with some notable exceptions. Contemporary contact detection approaches can be broadly categorized into two groups:

1. Learning-based approaches: Employment of machine learning techniques, either supervised or unsupervised, to estimate the contact state.
2. Model-based approaches: Definition of a deterministic model of the system by exploiting the contact dynamics.

Moreover, the aforementioned categories either directly employ the measured ground reaction wrenches by using a dedicated F/T sensor or they incorporate kinematics and dynamics to estimate the Ground Reaction Forces (GRFs). In the next two sections, the most frequently deployed approaches for dealing with contact estimation are outlined.

### 2.1 Simple Threshold

By far the simplest and most widely used approach is to threshold empirically the vertical GRF. The main underlying idea is, instead of assuming that the contact is stable, one can either measure or estimate the vertical GRF and define an empirical threshold to binary classify the contact state. This threshold is robot and controller dependent. The former is due to the fact that the mass of each platform is different and thus the measured GRF will be larger for heavier robots. The controller dependence is a direct consequence of the intensity of the exerted force from the robot to the ground. Aggressive gaiting induces large impacts between the feet

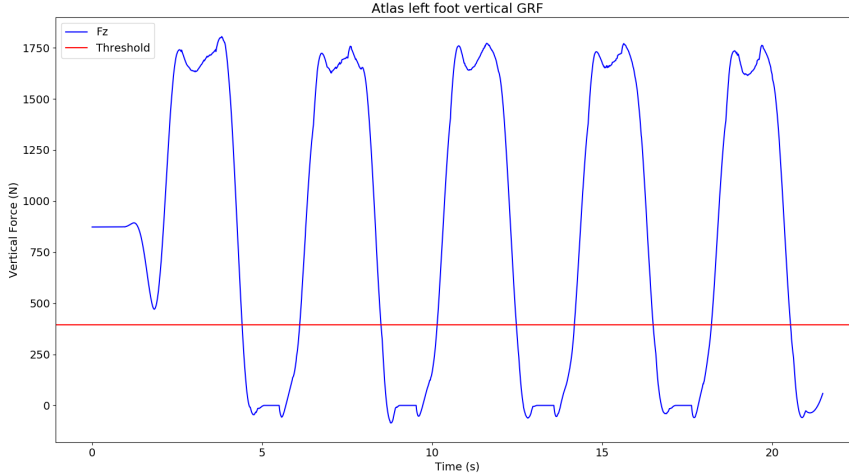


Figure 2.1: Smoothed vertical ground reaction force of Atlas’ left foot for five steps with **simple threshold**

and the ground resulting in greater reaction forces. In Fig. 2.1, the smoothed vertical GRF for five consecutive steps of the left foot of the Atlas simulated humanoid robot is illustrated with blue color. The vertical red line represents the threshold which is set, in this case, at  $390N$  to also include the double support phase. So, in every time stamp that the vertical GRF (blue line) is greater than the threshold (red line), the contact is categorized as stable which is a valid classification under the assumption that there is enough friction to prevent slippage. However, this heuristic is deemed to fail in cases where a foot slips and yet the vertical GRF is larger than the employed threshold. The latter inevitably leads to catastrophic results, and thus calls for more sophisticated approaches for contact state estimation. In the majority of instances, when developing a controller or a state estimator, this approach is typically employed owing to its straightforwardness and rapid implementation. Throughout this thesis, the aforementioned approach is utilized as a baseline and will be referred to as the ”**Simple Threshold**”.

## 2.2 Schmidt-Trigger

Another widely-used thresholding approach coined as *Schmidt-Trigger*, is considered as slightly more advanced alternative to *Simple Thresholding* as described in the previous section. *Schmidt-Trigger* relies on hysteresis thresholding with two thresholds (Fig. 2.2), namely a low and a high vertical GRF threshold. The core principle guiding the classification of the contact is as follows: When the GRF measurement is below the low limit, it is classified as unstable. When it is greater than the high limit it is considered stable and, finally, when it lies between the

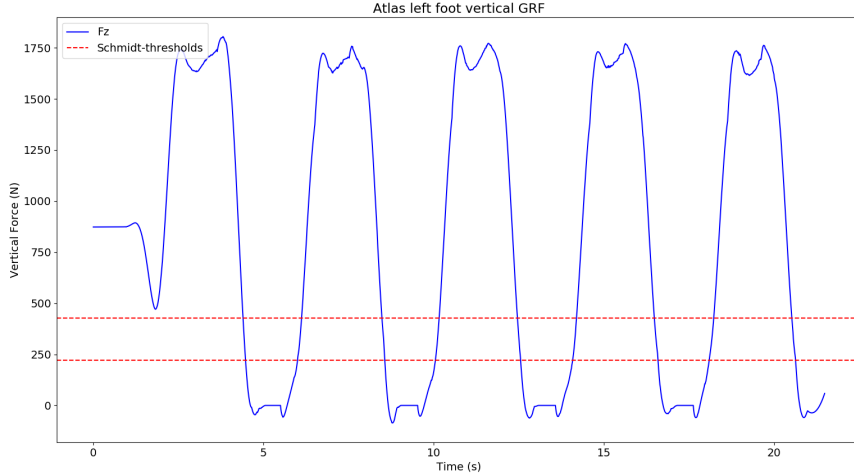


Figure 2.2: Smoothed vertical ground reaction force of Atlas' left foot for five steps with **Schmidt-Trigger**

two limits it is classified as the same class as the previous classification. The main advantages over simple thresholding are, the robustness against outliers that occur due to disturbances (force fluctuations) and an overall smoother representation of the contact states. The latter owns to the fact that the threshold is not a rigid boundary, and measurements near the lower limit are more likely to be classified as unstable. Although this approach is more sophisticated, it encounters similar shortcomings as simple thresholding while it also fails to detect slippage when the vertical GRF assumes large values.

## 2.3 State-of-the-art

### 2.3.1 Model-based approaches

Bloesch *et al.* [30] proposed a state estimation framework that fuses inertial measurements with leg kinematics by employing an Extended Kalman Filter (EKF). The absolute position of each foothold is included in the state vector and the contact classification occurs by determining whether the pose of the foot is constant. Capitalizing on this work, the same group extended their research [31] by substituting the EKF with an Unscented Kalman Filter and reformulating the state vector to be expressed in the base frame. In order to robustify the filter, they also introduced an outlier rejection method in the update step. They evaluated their approach on a StarLETH quadruped robot, proving its robustness to a certain amount of foot slippage. Towards this direction, in [32] a linear Kalman Filter is

utilized to estimate each leg state (swing or contact) for quadruped robots. The latter employs Gaussian probabilistic models for the contact forces and the terrain's ground height to infer the gait-phase. Although a very high estimation accuracy is recorded, the scheme relies on prior knowledge from pre-planned contacts and gait-phases and thus directly couples the control and estimation processes. Hwangbo *et al.* [33] estimated the GRFs by exploiting kinematic and dynamic models. They introduced a one-dimensional probabilistic framework to binary classify the contact state which is exported from a Hidden Markov Model that takes advantage of kinematics, differential kinematics and dynamics. This approach does not rely on F/T sensors, but effectively exploits joint position, velocity, and torque measurements to estimate the GRFs. In [1, 34], a Schmitt-trigger is utilized (Section 2.2) to classify the measured vertical GRFs from a F/T sensor mounted on the feet of an Atlas humanoid robot. Once the contact state is determined, they decide which leg should be used for state estimation. Similarly, in [35], the contact status of a quadruped robot is inferred from the GRFs by thresholding the robot dynamics. Finally, Focchi *et al.* [36], utilized the differential kinematics of a simulated quadruped robot on the velocity level. They directly compared the relative velocity between each foot and the base to detect and recover stability in slippage events. Moreover, they exploited the contact state transition in order to extract a rough estimate of the kinetic friction coefficient which is later used not only for recovering from slippage but also preventing it. However, this approach has never been tested in a real-world scenario.

### 2.3.2 Learning-based approaches

Rotella *et al.* [3] proposed an unsupervised learning framework that employs F/T and IMU measurements to perform clustering using fuzzy c-means. The sensors were mounted on the feet of a humanoid robot and they estimated the probability of contact for each one of the six Degrees of Freedom (DoFs) of the end effector. Moreover, the authors used the obtained contact probabilities in base estimation by adapting accordingly the kinematic measurement uncertainty. Likewise, in [37] the authors approach the quality of contact prediction by using unsupervised learning. In order to estimate the contact state, they measured the static friction coefficient by using haptic exploration of the ground with the robot's feet. Unsupervised learning was also employed to estimate the gait-phase probability in [38]. The authors utilized solely proprioceptive sensing, namely, joint encoders, IMU and F/T, and prior to clustering, they performed Principal Component Analysis (PCA) in order to reduce the dimensionality of the data and extract a more compact representation. A high accuracy for all three gait-phases was demonstrated with a simulated Valkyrie robot, but only stable walking was examined.

Contemporary supervised learning based approaches have been shown efficient in practice, but they require ground truth labels during the training process. Camurri *et al.* [39], used a one-dimensional logistic regression framework in order to specify dynamic GRF thresholds. More specifically, this one-dimensional classifier

utilized the estimated GRF from dynamics, joint position, and torque measurements to encode different GRF thresholds for different type of gaits. The learnt threshold was applied only on the vertical GRF while the other components were ignored under the assumption of sufficient friction to prevent slippage. Nevertheless, to perform the training, the ground-truth base velocity is needed. Recently, Lin *et al.* [40] introduced a deep convolutional neural network that utilizes IMUs and joint encoders to classify individual contacts as stable/unstable ones. Their approach was assessed on a Mini Cheetah robot and across various terrains where they reported an overall 97% accuracy. Despite the fact that the results indicate high classification accuracy, the framework is coupled with a specific robot and controller and it is unable to generalize to different platforms without new ground-truth labeled data. On the contrary, Ortenzi *et al.* [41] proposed an approach to estimate the contact constraints the robot experiences with the environment based only on joint position measurements.

Most of the aforementioned approaches from contemporary literature focus on classifying the contact as a binary state, with some notable exceptions such as [3, 37]. In order to exploit maximum information regarding the state of a foot, the contact state should not be treated as a categorical variable (contact/no contact), but rather as a continuous one. In many scenarios in uneven and/or slippery terrains, it is possible for a foot to be in touch with the ground regardless of the fact that the contact is unstable, giving rise to devastating consequences if this is not taken into account during locomotion.



## Chapter 3

# Significance of Contact State Estimation

This chapter explores the crucial role of contact state estimation in base state estimation, CoM estimation and bipedal locomotion. In Section 3.1, we describe how the knowledge of the contact state enhances legged odometry’s pose estimates and how it affects the over-time drift. Following that, in Section 3.2, we introduce the mathematical modelling of bipedal locomotion and how the contact state is embedded in the equations that describe the time evolution of the dynamic system.

### 3.1 Base State Estimation

Base State Estimation serves as a broad term encompassing all types of mobile robots, including legged robots. In the context of legged robots, it is occasionally referred to as ”legged odometry” without any loss of its intended significance. Legged odometry based on proprioceptive sensing refers to estimating the position and motion of a legged robot by solely utilizing internal sensor measurements, such as joint encoders and IMUs without relying on external visual or depth sensors. This approach is particularly useful in situations where visual information is limited or unreliable, such as in low-light environments or when dealing with occlusions.

In the realm of legged robots, contact state estimation holds immense significance. Legged robots operate by making and breaking contacts with the ground or other surfaces to achieve stable locomotion. Accurately estimating the contact state is essential in order to determine when and where the robot’s legs are in contact with the ground and if the foot in contact is ready to support weight. This information is crucial for various reasons. First, it helps in determining the robot’s support polygon, which aids in maintaining stability during locomotion. Second, it enables the robot to plan and execute appropriate foot placements, ensuring secure and balanced movements.

The success of legged odometry heavily relies on the accurate estimation of the

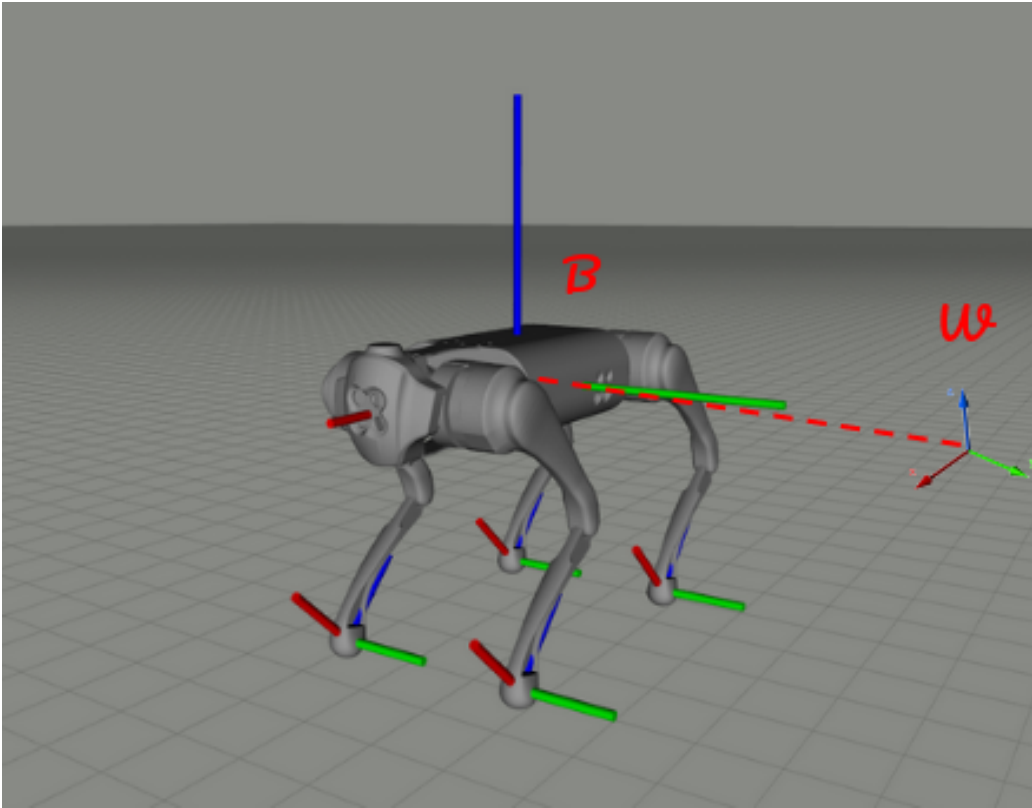


Figure 3.1: Simulated GO1 quadruped robot with base, foot and world frames

contact state. Incorrect or imprecise estimation can lead to errors in motion tracking and pose estimation, ultimately compromising the robot's stability and overall performance. By precisely acquiring the contact state, the legged odometry system can effectively incorporate the information into its motion estimation algorithms, resulting in more reliable and robust navigation. Moreover, accurate contact state estimation enables legged robots to dynamically adjust their gait patterns, control strategies, and stability mechanisms, enhancing their adaptability and agility in complex and dynamic environments. Thus, contact state estimation plays a pivotal role in enabling legged robots to achieve accurate odometry and successfully traverse challenging terrains.

In Fig. 3.1, a simulated quadruped robot is depicted alongside with the base, world and feet frames. The goal of base state estimation is to estimate the position and orientation of the base frame with respect to an inertial frame of reference (world frame). In the case when one of the feet is rotating Counter Clock Wise (CCW), according to the respective joint encoder readings, either the foot is moving backward or the base forward. When the contact state is unknown, it is impossible to deterministically state which one of the possible actions occurs. Without knowing if the aforementioned constraint is satisfied, the update of the

base estimate is unfeasible. Furthermore, the accuracy of the kinematic measurements will be compromised, resulting in the failure of any module that relies on them.

To this end, most approaches assume that the contact is fixed with the ground and slippage doesn't occur. This is a key assumption for base state estimation since it enables the constraining of the relative pose between the foot and the ground. The aforementioned assumption is essential for updating the state when the estimation relies solely on proprioceptive sensing. Although this assumption is valid most times, even a small dynamic contact event will result in drifting estimates over time or a spontaneous error spike if the foot velocity is significant. For example, during gaiting in an unstructured environment, the robot might step on small objects that will shift the desired foot position. Consecutively small undetected foot displacements will result in enormous drifts over time and finally track loss.

## 3.2 Bipedal Locomotion & CoM Estimation

One way of describing the dynamics of a rigid body (or in this case a bipedal robot) is by employing the Newton-Euler equations of motion. These consist of two parts, the linear and angular or Newton and Euler respectively. This mathematical formulation is widely used in the literature for CoM estimation and bipedal locomotion. In figure 3.2, a bipedal robot is depicted alongside with the friction cones of each contact points to assist in the visualization of the following mathematical formulation. Note that these equations are always expressed in an world frame.

### Linear Motion

When there are not any external forces applied to the robot and under the assumption that the mass of the robot is concentrated at the CoM, the linear equation of motion for a rigid body that is in contact with the ground can be modelled according to Newton's second law of motion:

$$m\ddot{\mathbf{c}} = m\mathbf{g} + \sum_i \mathbf{f}_i \quad (3.1)$$

where  $m$  is the total mass of the robot,  $\ddot{\mathbf{c}} = [\ddot{c}^x, \ddot{c}^y, \ddot{c}^z]^T$  is the center of mass acceleration,  $\mathbf{g} = [0, 0, -g^z]^T$  is the gravity acceleration vector and  $\mathbf{f}_i \in \mathbb{R}^3$  are the 3D ground reaction forces that are applied at the contact point  $i$ . Notice that there are no friction forces in (3.1) because they are incorporated in  $f_i^x$  and  $f_i^y$ .

### Angular Motion

The part that describes the angular dynamics is formulated as:

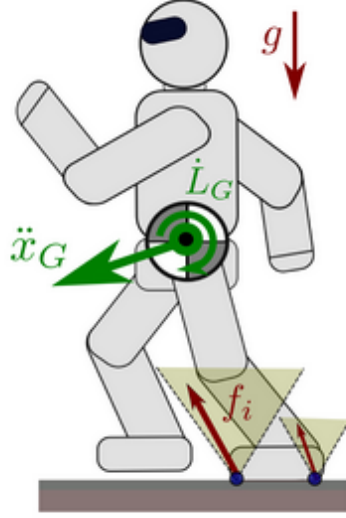


Figure 3.2: Humanoid robot walking [2]

$$\dot{\mathbf{L}} = \boldsymbol{\tau} = \sum_i (\mathbf{s}_i - \mathbf{c}) \times \mathbf{f}_i \quad (3.2)$$

where  $\dot{\mathbf{L}}$  is the angular momentum rate,  $\mathbf{s}_i$  are the contact points and  $\mathbf{c}$  is the position of the center of mass. The vector  $(\mathbf{s}_i - \mathbf{c})$  starts from contact point  $\mathbf{s}_i$  and ends at the Center of Mass. So,  $(\mathbf{s}_i - \mathbf{c}) \times \mathbf{f}_i$  is the torque that the contact force  $\mathbf{f}_i$  at  $\mathbf{s}_i$  generates to the CoM.

### Adding External Forces

When a robot interacts with the environment, external forces are usually applied to the robot and it is essential to be included in the dynamic model described in the previous section. So by adding external forces at (3.1) we will get:

$$m\ddot{\mathbf{c}} = m\mathbf{g} + \mathbf{f}_e + \sum_i \mathbf{f}_i \quad (3.3)$$

We multiply the above equation by the cross product of  $\mathbf{c}$ :

$$m\mathbf{c} \times \ddot{\mathbf{c}} = m\mathbf{c} \times \mathbf{g} + \mathbf{c} \times \mathbf{f}_e + \sum_i \mathbf{c} \times \mathbf{f}_i \quad (3.4)$$

And by reorganizing:

$$m\mathbf{c} \times (\ddot{\mathbf{c}} - \mathbf{g}) = \mathbf{c} \times \mathbf{f}_e + \sum_i \mathbf{c} \times \mathbf{f}_i \quad (3.5)$$

Now by adding (3.5) to (3.2) we get:

$$m\mathbf{c} \times (\ddot{\mathbf{c}} - \mathbf{g}) + \dot{\mathbf{L}} = \mathbf{c} \times \mathbf{f}_e + \sum_i \mathbf{c} \times \mathbf{f}_i + \sum_i (\mathbf{s}_i - \mathbf{c}) \times \mathbf{f}_i \quad (3.6)$$

or

$$m\mathbf{c} \times (\ddot{\mathbf{c}} - \mathbf{g}) + \dot{\mathbf{L}} = \mathbf{c} \times \mathbf{f}_e + \sum_i \mathbf{s}_i \times \mathbf{f}_i \quad (3.7)$$

In order to find the accelerations, we need to solve equation (3.7) for  $\ddot{c}^x$  and  $\ddot{c}^y$ . First, we need to calculate every term of Eq. (3.7).

$$\mathbf{c} \times (\ddot{\mathbf{c}} - \mathbf{g}) = \begin{bmatrix} c^y(\ddot{c}^z + g^z) - c^z\ddot{c}^y \\ c^z\ddot{c}^x - c^x(\ddot{c}^z + g) \\ c^x\ddot{c}^y - c^y\ddot{c}^x \end{bmatrix} \quad (3.8)$$

$$\dot{\mathbf{L}} = \begin{bmatrix} \dot{L}^x \\ \dot{L}^y \\ \dot{L}^z \end{bmatrix} \quad (3.9)$$

$$\mathbf{c} \times \mathbf{f}_e = \begin{bmatrix} c^y f_e^z - c^z f_e^y \\ c^z f_e^x - c^x f_e^z \\ c^x f_e^y - c^y f_e^x \end{bmatrix} \quad (3.10)$$

$$\mathbf{s}_i \times \mathbf{f}_i = \begin{bmatrix} s_i^y f_i^z - s_i^z f_i^y \\ s_i^z f_i^x - s_i^x f_i^z \\ s_i^x f_i^y - s_i^y f_i^x \end{bmatrix} \quad (3.11)$$

By substituting (3.8)-(3.11) in (3.7) and solving for  $\ddot{c}^x$  and  $\ddot{c}^y$  we get the following two equations for the  $\hat{x}$  and  $\hat{y}$  directions:

$$\ddot{c}^x = \frac{1}{mc^z} \left( mc^x(\ddot{c}^z + g^z) + \dot{L}^y - c^x f_e^z + c^z f_e^x - \sum_i s_i^x f_i^z + \sum_i s_i^z f_i^x \right) \quad (3.12)$$

$$\ddot{c}^y = \frac{1}{mc^z} \left( mc^y(\ddot{c}^z + g^z) + \dot{L}^x - c^y f_e^z + c^z f_e^y - \sum_i s_i^y f_i^z + \sum_i s_i^z f_i^y \right) \quad (3.13)$$

Also by solving (3.1) we can get the  $z$ -component of the acceleration:

$$\ddot{c}^z = \frac{1}{m}(f_N + f_e^z) - g^z \quad (3.14)$$

with  $f_N \triangleq \sum_i f_i^z$ , the vertical ground reaction force. Finally, we substitute  $\ddot{c}^z$  from (3.14) into (3.12) and (3.13):

$$\ddot{c}^x = \frac{1}{mc^z} \left( c^x f_N + c^z f_e^x - \dot{L}^y + \sum_i s_i^z f_i^x - \sum_i s_i^x f_i^z \right) \quad (3.15)$$

$$\ddot{c}^y = \frac{1}{mc^z} \left( c^y f_N + c^z f_e^y + \dot{L}^x + \sum_i s_i^z f_i^y - \sum_i s_i^y f_i^z \right) \quad (3.16)$$

The above equations can be utilized either to estimate the CoM acceleration or as a control input to achieve the desired accelerations. The only problem is that  $f_i^x$  and  $f_i^y$  can not be measured directly since the friction resistance force is incorporated in them. In order to overcome this limitation, we make a **key assumption: The foot doesn't slip**. This assumption enables the elimination of the  $x - y$  plane forces since they cancel out with friction and thus,  $f_i^{x,y} = 0$  for every contact point  $i$ .

$$\ddot{c}^x = \frac{1}{mc^z} \left( c^x f_N + c^z f_e^x - \dot{L}^y - \sum_i s_i^x f_i^z \right) \quad (3.17)$$

$$\ddot{c}^y = \frac{1}{mc^z} \left( c^y f_N + c^z f_e^y + \dot{L}^x - \sum_i s_i^y f_i^z \right) \quad (3.18)$$

Finally, we define the Center of Pressure (CoP) as:

$$p^x = \frac{\sum_i s_i^x f_i^z}{\sum_i f_i^z} = \frac{\sum_i s_i^x f_i^z}{f_N}, \quad f_N > 0 \quad (3.19)$$

$$p^y = \frac{\sum_i s_i^y f_i^z}{\sum_i f_i^z} = \frac{\sum_i s_i^y f_i^z}{f_N}, \quad f_N > 0 \quad (3.20)$$

By using the CoP definition and refactoring (3.17) and (3.18) we get the final equations:

$$\ddot{c}^x = \frac{c^x - p^x}{mc^z} f_N - \frac{\dot{L}^y}{mc^z} + \frac{1}{m} f_e^x \quad (3.21)$$

$$\ddot{c}^y = \frac{c^y - p^y}{mc^z} f_N + \frac{\dot{L}^x}{mc^z} + \frac{1}{m} f_e^y \quad (3.22)$$

$$\ddot{c}^z = \frac{1}{m} (f_N + f_e^z) - g^z \quad (3.23)$$

Equations (3.21)-(3.23) effectively model the motion of a legged robot and are the foundation upon which, many controllers and estimators are based on to describe the dynamics of the system. These equations were derived under the assumption that the contact is stable. When this assumption is false, unmodelled dynamics are encountered which will result in devastating consequences for the robot's stability and controllability.

## Chapter 4

# Robust Contact State Estimation in Humanoid Walking Gaits

In this chapter, we introduce a deep learning framework based on proprioception, specifically a F/T and an IMU sensor in each leg, to determine the contact state probabilities, namely stable or slip/no contact probabilities for dynamic walking gaits over variable friction surfaces that can further benefit the legged locomotion problem. Our contribution to the state-of-the-art regards:

- A supervised approach for contact detection. We demonstrate that a model trained with walking gaits over a specific friction coefficient, generalizes to a very large range of frictions. Additionally, the model also generalizes to different robotic platforms. Although our model is trained with the ATLAS robot, the same model provides highly accurate contact estimation in NAO and TALOS walking gaits.
- A framework that relies solely on proprioceptive sensing that is readily available in contemporary humanoids.
- A demonstration that, although the model is trained in simulation with the ground-truth contact states as labels, it can be employed to infer the contact state with a real TALOS humanoid.
- A framework that has been extensively evaluated against state-of-the-art approaches in contact estimation and its efficiency is demonstrated both in simulation and real robot experiments.
- The release of an open-source module implementation in ROS/Python, named Legged Contact Detection (LCD) module [42].

We directly compare our approach with [3], since IMUs and F/T in the legs are also considered. In this case a shortcoming is that 12 fuzzy c-means clustering

models must be individually trained, one for each of the three translational and rotational DoFs of both legs, to collectively estimate the feet contact states.

In this work we follow a radically different approach. Firstly, we consider data to be received by F/T and IMU sensors in the robot’s feet. Secondly, we explore contact model training using a single robot (e.g., ATLAS) in simulation for just a single surface friction value. Our data collection and training method: 1) achieves highly accurate and robust surface contact detection, 2) generalizes the contact estimation to surfaces of friction that were not in the training dataset, 3) generalizes well in different simulated robotic platforms (from light to heavy weighted), and 4) can be applied directly to real-robots. We, thus, propose a novel friction- and robot- invariant method for accurate and robust contact estimation, based only on GRF and IMU sensory data.

## 4.1 Training Data Acquisition

Training data is an important aspect of machine learning. Instead of blindly employing all available sensory data in a training session, we provide a physical interpretation to a particular choice of features that are directly correlated to the contact state. The datasets used for LCD training and testing are released in [42].

### 4.1.1 Contact State in the Centroidal Dynamics

The centroidal dynamics of a humanoid during locomotion can be described by the Newton-Euler equations as described in the previous chapter:

$$m(\ddot{\mathbf{c}} + \mathbf{g}) = \sum_i \mathbf{f}_i \quad (4.1)$$

$$m\mathbf{c} \times (\ddot{\mathbf{c}} + \mathbf{g}) + \dot{\mathbf{L}} = \sum_i \mathbf{s}_i \times \mathbf{f}_i + \boldsymbol{\tau}_i \quad (4.2)$$

where  $\mathbf{c}$  and  $\ddot{\mathbf{c}}$  are the CoM position and acceleration,  $\dot{\mathbf{L}}$  is angular momentum rate around the CoM,  $\mathbf{f}_i$  and  $\boldsymbol{\tau}_i$  are the Ground Reaction Forces (GRFs) and Torques (GRTs),  $\mathbf{s}_i$  are the contact points,  $\mathbf{g}$  is the gravity vector, and  $m$  is the robot’s mass.

Subsequently, in order for a leg to maintain contact and neither slip nor rotate, the friction constraints must apply:

$$\sqrt{(f_i^x)^2 + (f_i^y)^2} \leq \mu^{x,y} f_i^z \quad (4.3)$$

$$-\tau_i^y / f_i^z \leq p^x \quad (4.4)$$

$$\tau_i^x / f_i^z \leq p^y \quad (4.5)$$

$$|\tau_i^z| \leq \mu^z f_i^z \quad (4.6)$$

where  $\mathbf{p}$  is the center of pressure and  $\mu^{x,y}, \mu^z$  are the planar and rotational contact friction coefficients, respectively.

As evident there is a direct correlation of the contact points and, thus, the contact state with the ground reaction wrenches and the centroidal dynamics. Although we can measure the left and right leg contact wrenches  ${}^l\mathbf{f}_l, {}^l\boldsymbol{\tau}_l$  and  ${}^r\mathbf{f}_r, {}^r\boldsymbol{\tau}_r$  with F/T sensors in the local leg frames and also compute the CoM velocity  ${}^b\dot{\mathbf{c}}$  and angular momentum rate  ${}^b\dot{\mathbf{L}}$  in the base frame with kinematics, friction depends on the environment and prohibits the analytical derivation of the contact state.

#### 4.1.2 Contact State in the Leg Kinematics

The contact state is also directly linked to the leg kinematics namely, the left and right leg spatial linear and angular velocities  ${}^l\mathbf{v}_l, {}^l\boldsymbol{\omega}_l$  and  ${}^r\mathbf{v}_r, {}^r\boldsymbol{\omega}_r$ . More specifically, for the left leg to experience a stable contact with the environment and not slip in the tangential directions, the following conditions must apply:

$${}^l f_l^z > 0 \quad (4.7)$$

$${}^l v_l^x = 0 \quad (4.8)$$

$${}^l v_l^y = 0 \quad (4.9)$$

$${}^l \omega_l^z = 0 \quad (4.10)$$

Furthermore, when the leg is stationary on the ground and is not breaking the contact by lifting nor rotating, then:

$${}^l v_l^z = 0 \quad (4.11)$$

$${}^l \omega_l^x = 0 \quad (4.12)$$

$${}^l \omega_l^y = 0 \quad (4.13)$$

Accordingly, the same conditions apply to the right leg.

In the above, the spatial rotational velocities  ${}^{l,r}\boldsymbol{\omega}_{l,r}$  can be directly measured with an IMU attached to the foot links. On the contrary, the spatial linear velocities  ${}^{l,r}\mathbf{v}_{l,r}$  cannot be measured and must be estimated. To avoid introducing correlations between the base and the contact state estimation, we employ the leg spatial linear accelerations  ${}^{l,r}\boldsymbol{\alpha}_{l,r}$ , which can also be measured by the leg IMUs.

## 4.2 Robust Contact Estimation with Deep Learning

To accurately infer the leg’s contact state we devised a supervised learning framework, termed Legged Contact Detection (LCD), depicted in Figure 4.1. The data employed for the training procedure were the leg F/T measurements, namely  ${}^l\mathbf{f}_l, {}^l\boldsymbol{\tau}_l$  and the leg IMU data, namely  ${}^l\boldsymbol{\omega}_l, {}^l\boldsymbol{\alpha}_l$ , as measured in the local leg frame. A single model is trained with the left and right leg F/T and IMU data and is used to infer the contact states for both legs.

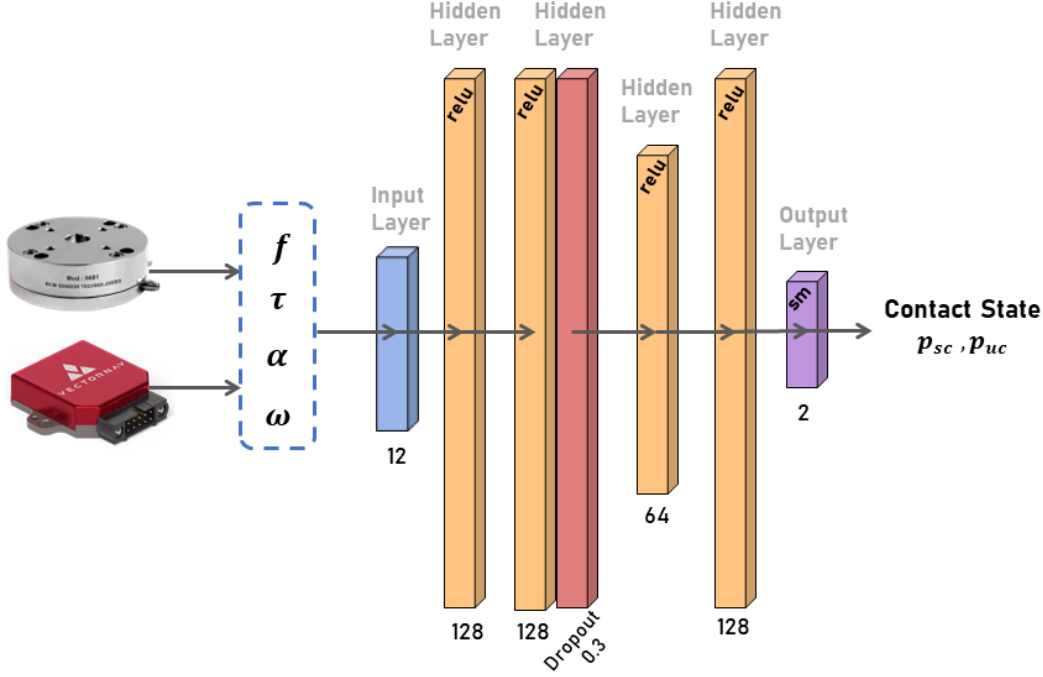


Figure 4.1: LCD Deep Learning Architecture.

#### 4.2.1 Preprocessing

For the F/T measurements the following model was considered:

$${}^l \mathbf{f}_l = {}^l \bar{\mathbf{f}}_l + \mathbf{b}_f + \mathbf{w}_f \quad (4.14)$$

$${}^l \boldsymbol{\tau}_l = {}^l \bar{\boldsymbol{\tau}}_l + \mathbf{b}_\tau + \mathbf{w}_\tau \quad (4.15)$$

where the  ${}^l \bar{\mathbf{f}}_l$ ,  ${}^l \bar{\boldsymbol{\tau}}_l$  are the true GRFs and GRTs,  $\mathbf{b}_f$ ,  $\mathbf{b}_\tau$  and  $\mathbf{w}_f$ ,  $\mathbf{w}_\tau$  are the F/T measurement biases and zero-mean Gaussian noises, respectively. Similarly, for the IMU measurements the following model was employed:

$${}^l \boldsymbol{\alpha}_l = {}^l \bar{\boldsymbol{\alpha}}_l + {}^l \mathbf{R}_w \mathbf{g} + \mathbf{b}_\alpha + \mathbf{w}_\alpha \quad (4.16)$$

$${}^l \boldsymbol{\omega}_l = {}^l \bar{\boldsymbol{\omega}}_l + \mathbf{b}_\omega + \mathbf{w}_\omega \quad (4.17)$$

where the  ${}^l \bar{\boldsymbol{\alpha}}_l$ ,  ${}^l \bar{\boldsymbol{\omega}}_l$  are the true linear acceleration and angular velocity,  ${}^l \mathbf{R}_w$  is the rotation from the world to the left leg frame,  $\mathbf{g}$  is the gravity vector,  $\mathbf{b}_\alpha$ ,  $\mathbf{b}_\omega$  and  $\mathbf{w}_\alpha$ ,  $\mathbf{w}_\omega$  are the IMU measurement biases and zero-mean Gaussian noises. Evidently, the same models apply for the right leg F/T and IMU measurements. During the data preprocessing all measurements exceeding  $3\sigma$  were identified as outliers and eliminated from the dataset.

All data have been normalized in each dimension with their maximum value to avoid large scale measurements such as the vertical GRF  ${}^l f_l^z$  dominating the

learning procedure. Subsequently, the absolute value was taken since slip is bidirectional and does not depend on measurement signs. Moreover, all data have been synchronized and downsampled to  $100Hz$  since the contact state commonly changes when the robot takes a step which contemporary humanoids accomplish with a slower rate, e.g.,  $1 - 2Hz$ .

## 4.2.2 Architecture

The LCD network, illustrated in Figure 4.1, consists of 2 hidden layers with 128 neurons followed by a 30% dropout layer to prevent overfitting. Subsequently, two more hidden layers were added with 64 and 128 neurons, respectively, to feed an output layer of 2 units, one for each contact probability, namely stable contact or unstable/no contact. For all hidden layers the ReLU activation was used, while for the output layer the sigmoid was employed to guarantee that the output is a valid probability. The overall architecture was determined experimentally while aiming to maximize the accuracy of the classifier on data acquired from other robotic platforms than the one employed for training. Hyperparameter grid search was performed to optimize the efficiency of the network. Overall, LCD was trained for 30 epochs, with a batch size of 16 and the *adam* optimizer.

Accordingly, we formulate a supervised classification problem by minimizing the binary cross-entropy loss:

$$L = -(y_{sc} \log(p_{sc}) + (1 - y_{sc}) \log(1 - p_{sc})) \quad (4.18)$$

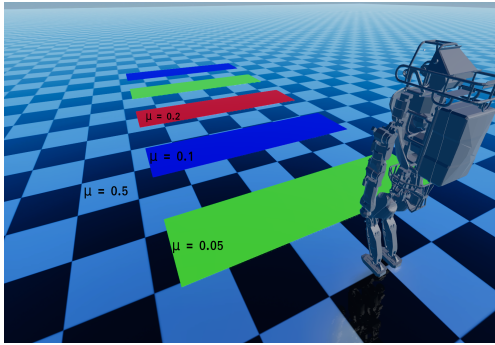
where  $p_{sc}$  is the stable contact probability,  $p_{uc} = 1 - p_{sc}$  is the unstable/no contact probability and  $y_{sc}$  is the ground truth stable contact label obtained by evaluating Eqs. (4.3) - (4.6) as well as Eqs. (4.8) - (4.13) in simulation, as also outlined in the next section.

## 4.3 Results

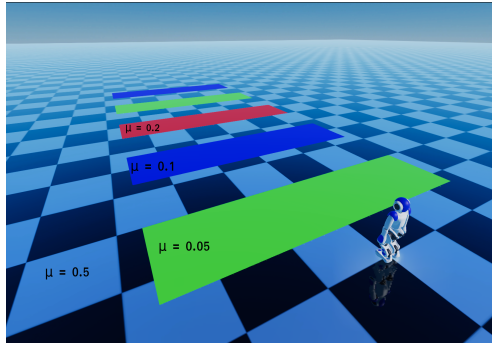
In the current section, we present quantitative and qualitative results that demonstrate the accuracy and efficacy of the proposed framework both in simulation and real world experiments. LCD was implemented in ROS/Python and is publicly available at [42]. A snapshot of the experimental setup is illustrated in Figure 4.2. In addition all of our experiments are presented in high resolution at <https://youtu.be/csUIadkT70M>.

### 4.3.1 Simulation Results

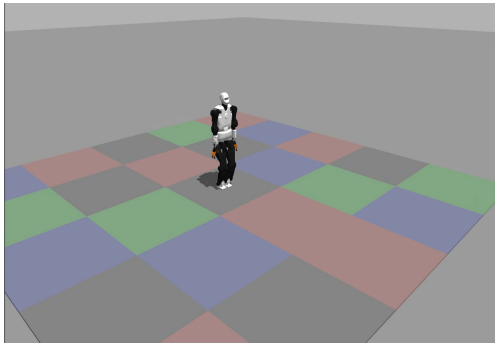
To conduct a quantitative and qualitative assessment, we employed an ATLAS and a NAO humanoid robot in RaiSim [43]—a high-accuracy multi-contact simulator for articulated robots— and the TALOS humanoid in Gazebo [44]. Accordingly, to generate walking patterns, we’ve implemented a robot generic omnidirectional walking motion planning [45] and a real-time gait stabilization module [46], both based on



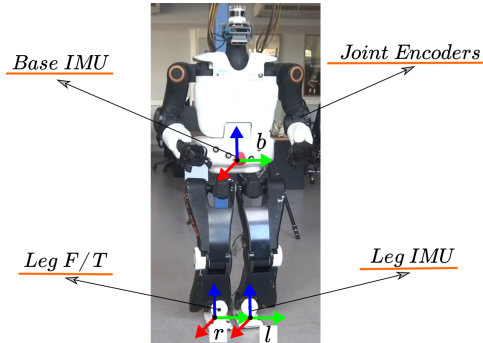
(a) Simulated ATLAS experimental setup



(b) Simulated NAO experimental setup



(c) Simulated TALOS experimental setup



(d) Real TALOS robot

Figure 4.2: Experimental setup for variable friction surfaces.

the Linear Inverted Pendulum (LIPM) dynamics [47, 48]. Subsequently, to realize the desired trajectories in each humanoid, we’ve also developed a real-time whole body control module [49] based on stack of tasks at the velocity level [50]. In our formulation, higher priority was given to the desired leg trajectories, then to the desired CoM position and torso orientation, and finally to a standing posture joint configuration task to maintain postural balance. Regarding the feedback of the motion planning, real-time stabilization and whole-body inverse kinematics, the ground-truth values were employed. The latter modules are also released as open-source ROS/C++ packages to reinforce further research endeavors.

Next, we’ve commanded each robot to continuously walk over multiple surfaces with varying friction coefficients from 0.05 to 1.2, for approximately 10 minutes, to record the needed dataset. Overall, the above sessions resulted in an average distribution of the labels as follows: 60% for Stable Contact (SC) and 40% for Unstable Contact (UC) (30% for no contact and 10% for slip). The legs’ IMU and F/T measurements were available at  $500Hz$  for ATLAS and TALOS and at  $100Hz$  for NAO. In all measurements, i.i.d Gaussian noise was added to provide realistic noise levels according to Table 4.1.

Subsequently, the LCD model is trained with a 10 minute omni-directional

walking gait via the ATLAS robot and over a 0.2 friction coefficient surface. This model is then used to infer the contact state for every walking gait performed with the ATLAS, NAO, and TALOS robot over variable friction surfaces. To compute the necessary training labels, we evaluate Eqs. (4.3)–(4.6) and Eqs. (4.8)–(4.13) using the ground-truth values at every discrete time instant. If the latter is true, the contact label is characterized as SC, otherwise it is a UC. Note that UC includes the slip and no contact states.

To quantitatively assess the proposed framework in terms of accuracy, we employ several state-of-the-art contact detection methods. More specifically, we have implemented a) the vertical GRF thresholding (T), b) the Schmidt Trigger [1] (ST), which relies on hysteresis thresholding with a low and a high vertical GRF threshold, and c) the fuzzy c-means (FCM) contact detector [3]. The first two are binary contact classification methods while the third is a contact probability detector based on leg F/T and IMU data clustering. The thresholds employed for each robot were finely tuned for each dataset to yield the best results, while for FCM the fuzziness parameter was set to 1.2 and a batch size of 20 input samples was used for all robots.

### 4.3.2 Comparison to Thresholding methods

The quantitative results (Table 4.2) from the comparison between LCD, T, and ST indicate that LCD outperforms every thresholding model in identifying the UC state. Although the difference is between 3-7%, this is rather significant because slip occurs rarely and for a short period of time and, thus, the no contact class dominates in size the UC labels. Figure 4.3 demonstrates how the vertical force of the left foot varies during gait and the ground truth labels for SC (1.0) and UC (0.0). The latter presents two rows whereby the top row refers to the basic thresholding methods, namely T and ST, and the bottom row presents our own results. The depicted gait pattern is extracted from the ATLAS robot while walking on surfaces with varying friction coefficients. Each peak represents a step,

Table 4.1: Simulation noise standard deviations.

	Continuous	Discrete (100Hz)
$\sigma_\alpha$	$0.0008m/s^2/\sqrt{Hz}$	$0.008m/s^2$
$\sigma_\omega$	$0.0005rad/s/\sqrt{Hz}$	$0.005rad/s$
$\sigma_{b_\alpha}$	$0.0001m/s^3/\sqrt{Hz}$	$0.001m/s^3$
$\sigma_{b_\omega}$	$0.0006rad/s^2/\sqrt{Hz}$	$0.006rad/s^2$
$\sigma_f$	$0.07N/\sqrt{Hz}$	$0.7N$
$\sigma_\tau$	$0.003Nm/\sqrt{Hz}$	$0.03Nm$
$\sigma_{b_f}$	$0.0001N/s/\sqrt{Hz}$	$0.001N/s$
$\sigma_{b_\tau}$	$0.0001Nm/s\sqrt{Hz}$	$0.001Nm/s$

Table 4.2: LCD evaluation on variable friction datasets

Dataset	LCD		Simple Threshold		Schmidt Trigger	
	SC(%)	UC(%)	SC(%)	UC(%)	SC(%)	UC(%)
ATLAS $\mu = 0.6$ (15k)	97	96	97	93	96	92
ATLAS random $\mu$ (50k)	96	84	95	79	94	81
NAO random $\mu$ (15k)	96	80	94	73	89	75
TALOS random $\mu$ (50k)	92	70	98	64	99	65

more specifically the first step is on terrain with  $\mu = 0.5$ , where  $\mu$  stands for the terrain-foot friction coefficient. Similarly, the second peak regards a case with  $\mu = 0.05$  (refers to walking on almost ice-like surfaces), and the third and fourth peaks refer to  $\mu = 0.1$  and  $\mu = 0.5$ , respectively. Note that the gait phase in the initial part of the first step (peak) and the final part of the last step is Double Support. It is interesting to observe that during the second step, although the robot has transferred its weight to perform the next step, the foot is slipping and hence T and ST are misclassifying the corresponding data points (purple region) since  ${}^lF_i^z$  is greater than the threshold. On the contrary, this is not the case with the proposed LCD framework, which identifies the UC state of the gait. Similar observations also hold true for the subsequent steps that are illustrated in the same figure.

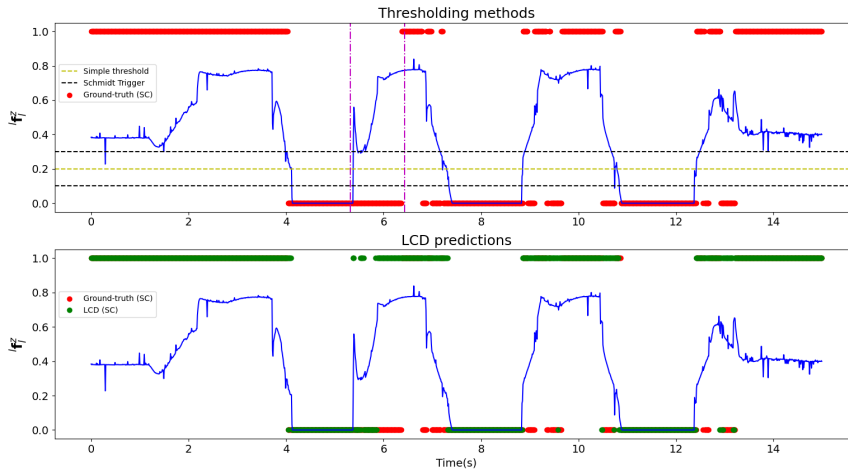


Figure 4.3: Thresholding and LCD predictions for SC on ATLAS walking gaits with varying friction coefficient surfaces

### 4.3.3 Comparison to unsupervised learning

In Figure 4.4 we demonstrate a qualitative comparison between unsupervised learning (FCM) and the proposed model (LCD) on the same gaits. The top graph illustrates the probability of stable contact ( $p_{sc}$ ) as computed by the FCM versus the ground truth labels. FCM accurately predicts the first step and, although it recognises the instability at the beginning of the second step, it quickly converges to the incorrect label. On the other hand, the bottom graph illustrates the predictions of LCD which successfully captures most of the data samples classified as UC (0.0) but also SC (1.0) according to the ground truth labels.

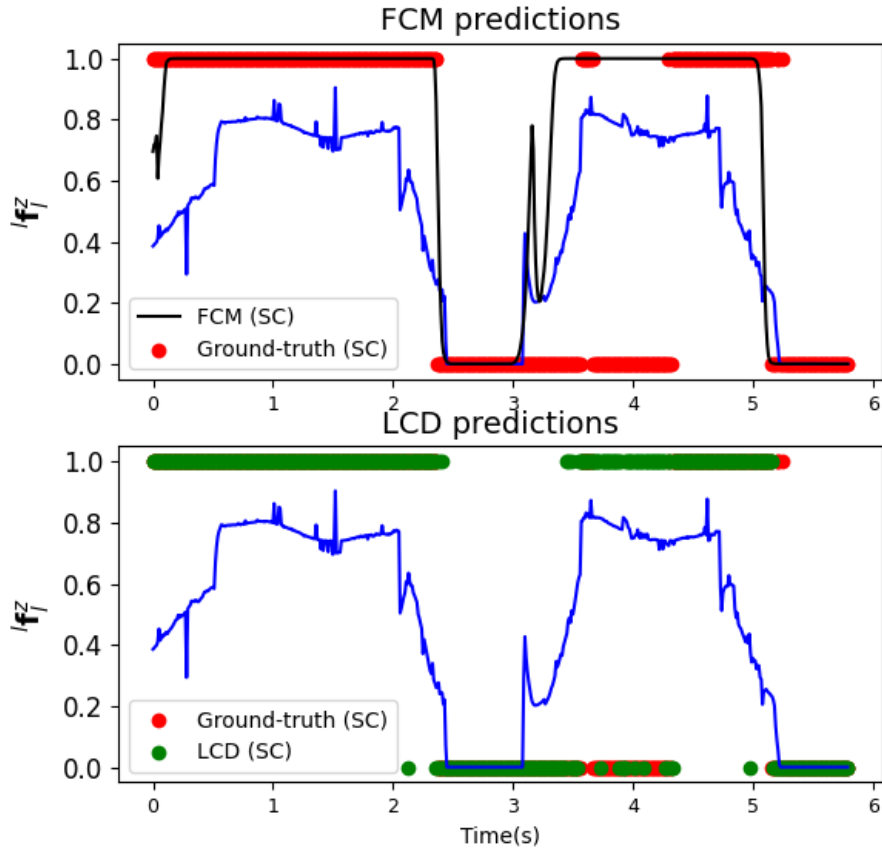


Figure 4.4: Unsupervised learning and LCD predictions on normal and low friction gaits.

#### 4.3.4 LCD with feature reduction

In order to test the robustness of LCD and its transferability to point feet robotic platforms (such as quadrupeds), we removed all the F/T measurements from the training dataset except the vertical force  $F_z$ . Next, we trained the model by using only  $F_z$  and IMU measurement. After training, the model was able to make successful predictions on test datasets with different but not extremely low friction coefficients, as shown in Table 4.3.

Table 4.3: LCD performance with reduced features

dataset	SC(%)	UC(%)
ATLAS, $\mu = 0.5$	91	98
ATLAS $\mu = 0.4$	92	99

#### 4.3.5 Experimental Results: Application to Base Estimation

Finally, we employed LCD to predict the stable contact state probability for an actual TALOS humanoid and facilitate base state estimation with the State Estimation Robot Walking (SEROW) framework [29]. The latter fuses effectively the contact state, kinematics, and the base IMU measurements to provide estimates for the base position, velocity and orientation. A vicon motion capture system was used to provide the ground-truth base pose every  $200Hz$ . Figure 4.5 illustrates the 3D-base position error over time, whereby a slight drift is observed in the  $x$  and  $z$  axes for this 60s gait. The measured root mean square error was particularly small, namely  $0.0245m$ ,  $0.0101m$ ,  $0.0123m$  for the base position and  $0.7058deg$ ,  $1.2035deg$ , and  $1.8426deg$  for the orientation, validating the employed stable contact state probabilities.

#### 4.3.6 Discussion

We have demonstrated that an LCD model trained on a single dataset with the ATLAS robot walking over specific friction surfaces in RaiSim, achieves highly accurate contact detection. Additionally, the model generalizes well to contact estimation a) over surfaces with variable friction not previously included in the training dataset, b) with different robotic platforms scaling from small size light-weight robots such as NAO to full size heavy robots such as TALOS, and c) with different simulation platforms namely RaiSim and Gazebo. Consequently, it is rather straightforward to claim that the LCD architecture ought to have captured some robust contact features which are invariant to friction and to robot characteristics such as weight and height. Subsequently, we presented that the same architecture provides accurate contact estimation only with the GRF and the IMU data as input. The latter implies that this method can be readily adopted for

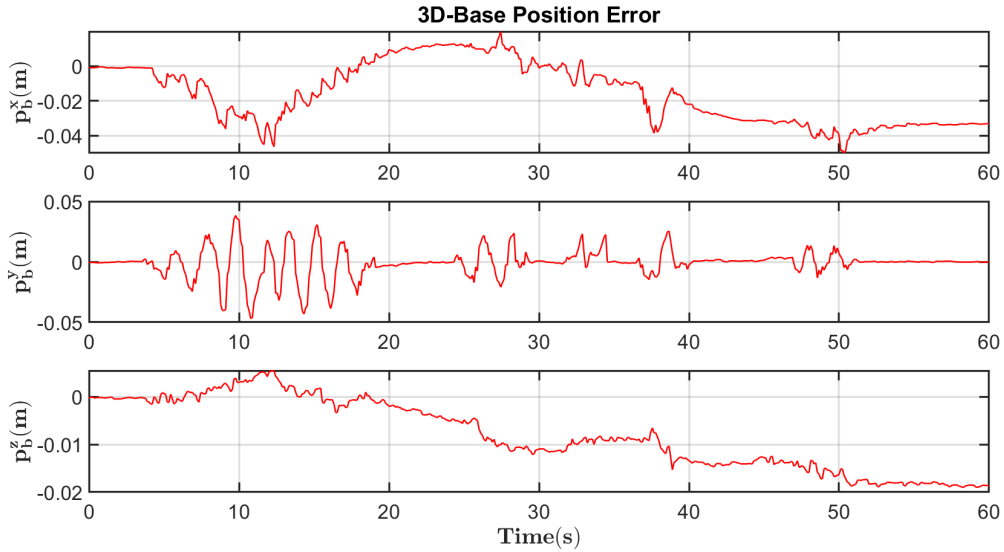


Figure 4.5: 3D-Base position error of the estimated base position with SEROW from the corresponding ground-truth base position.

robots with point feet, such as modern quadruped robots. These results pave the way for a holistic contact detection mechanism that is robot and contact agnostic.

## 4.4 Conclusions

In this chapter we introduced LCD, a supervised deep learning framework that provides a solution to contact detection by accurately and robustly estimating the leg contact state based solely on proprioceptive sensing. Although the latter rely on simulated ground-truth contact data for the training process, LCD generalizes across robotic platforms and can be readily transferred from simulation to real world setups. To reinforce further research endeavours we released LCD as an open-source ROS/Python package [42].

Finally, we have shown that contact invariant features exist between different robotic platforms that can further facilitate the contact estimation problem. LCD has been experimentally validated in terms of accuracy in simulation and has been compared against state-of-the-art approaches for contact detection with a simulated ATLAS, TALOS, and NAO robot. Additionally, its efficacy has been demonstrated in base estimation with an actual TALOS humanoid.



## Chapter 5

# Probabilistic Contact State Estimation for Legged Robots using Inertial Information

In this chapter we present yet another novel contact state estimation approach that, unlike the approach presented in the previous chapter, it does not rely on F/T measurements and also does not require ground truth data and labels. According to the Coulomb’s model for dry friction (Eq. 5.3), the contact state depends directly on the Ground Reaction Force (GRF) and the friction coefficient between the foot and the ground. The former is typically acquired directly from a F/T sensor while the latter needs to be experimentally measured either by a human or a dedicated sensor. Often these sensors are impractical due to various reasons. For example, reliable force sensors are expensive and tend to degrade over repetitive use, as consequence of high speed motions and large impact wrenches. For the particular case of quadruped robots a further limitation regards the sensor’s mass. An average F/T sensor weights 100 g, thus accounting of approximately 50% of the overall leg inertia, resulting to reduced acceleration capability [33].

In this model-based approach, we utilize only inertial information, more specifically, an IMU mounted on each individual foot of the robot. We explore the dynamics of the contact event and by capitalizing on the uncertainty of the sensor measurements, we are able extract the stable contact probability. Moreover, we treat the contact state as a six Degrees of Freedom (DoF) continuous variable and estimate each individual contact probability which is then fused into the final estimation. Our main contributions can be summarized as follows:

- To the best of our knowledge this is the first work that estimates the contact probability by considering solely inertial measurements.
- The proposed stable contact detection module is robot agnostic. In other words, it can be employed on any legged robot that is equipped with mid-range IMUs mounted on its feet. By executing a few steps on a surface with

sufficient friction (ensure stable contact), the module can trivially be fine tuned for the employed robotic platform.

- To further facilitate and promote research in the sector, both the code and the datasets that the proposed method was tested upon are released as an open-source project at [51].

## 5.1 Problem Formulation

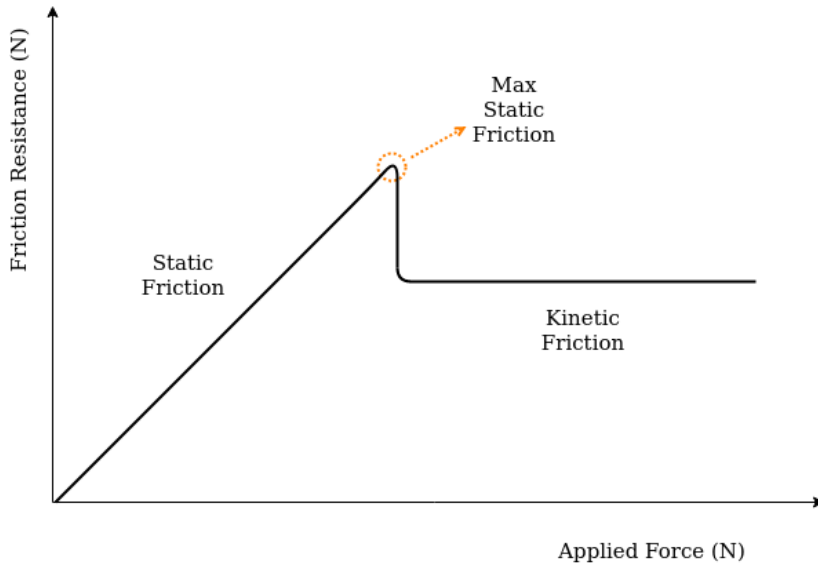


Figure 5.1: Static and Kinetic friction force.

### 5.1.1 Background

Static friction is the force that prevents an object from moving when the relative speed between the object and the supporting surface is zero. Frictional force offers the resistance to the applied force opposing its motion:

$$T_s = \mu_s F_z \quad (5.1)$$

where  $T_s$  is the static friction force,  $\mu_s$  is the static friction coefficient and  $F_z$  is the normal to the plane GRF. On the contrary, when an object is moving and is in touch with a surface, the resisting force is the kinetic friction  $T_k$ :

$$T_k = \mu_k F_z \quad (5.2)$$

where  $\mu_k$  is the kinetic friction coefficient. As a general rule,  $\mu_k$  is smaller than  $\mu_s$  and hence  $T_k < T_s$ , indicating that once the object starts moving it is harder to

stop because the resistance friction force is smaller. Although most contemporary approaches assume that the friction force is constant, in practice this is not the case. In Fig. 5.1, we depict how the resistance force varies when the applied force assumes larger values. In legged robot locomotion, when the threshold of motion is surpassed, the resistance force instantly reduces and the foot begins to accelerate for a certain period of time until either the robot loses balance entirely or deceleration occurs and the foot comes to rest. Although it is possible for an object to be moving with constant velocity ( $a_x = a_y = a_z = 0 \text{ m/s}^2$ ) when the applied and resistance forces are equal, for the reasons stated previously it is infeasible to occur on the robot's foot during dynamic locomotion. Consequently, we explore the cases when the foot is completely still or it accelerates after the threshold of motion is surpassed.

According to the Coulomb's model for dry friction, in order for a contact to be classified as stable, i.e. the relative speed between two objects in contact is zero, the following condition must hold true:

$$\sqrt{F_x^2 + F_y^2} \leq \mu_s F_z, \quad F_z > 0 \quad (5.3)$$

where  $F_x$  and  $F_y$  are the lateral forces at each contact point. Although in physics Eq. (5.3) describes the contact state deterministically (stable or unstable), a problem arises during impact when vibrations occur between the foot and the ground while simultaneously the robot transfers its weight towards the support leg. These fluctuations between the two terms of Eq. (5.3), namely  $\sqrt{F_x^2 + F_y^2}$  and  $\mu_s F_z$ , are illustrated in Fig. 5.2, where if the blue line is greater than the red one, the contact is considered stable otherwise unstable. As can be observed, during impact the contact state oscillates between stable and unstable until the robot transfers its weight and the absolute difference between the two terms becomes significant. Accordingly, in this work we aim at detecting this part of the gait phase as will be illustrated in the experimental results section.

### 5.1.2 Measurement Model

Similarly to the previous work (Chapter 4), the following model was considered for the IMU measurements:

$$\boldsymbol{\alpha}^f = \bar{\boldsymbol{\alpha}}^f + {}^f\mathbf{R}_w \mathbf{g} + \mathbf{b}_\alpha + \mathbf{w}_\alpha \quad (5.4)$$

$$\boldsymbol{\omega}^f = \bar{\boldsymbol{\omega}}^f + \mathbf{b}_\omega + \mathbf{w}_\omega \quad (5.5)$$

where  $\boldsymbol{\alpha}^f \in \mathbb{R}^3$  and  $\boldsymbol{\omega}^f \in \mathbb{R}^3$  are the linear acceleration and angular velocity measurement vectors for the corresponding foot as measured by the IMU in the local foot frame, respectively. For a humanoid,  $f \in \{L, R\}$  (left or right), while for a quadruped  $f \in \{RL, RR, FL, FR\}$  (rear left, rear right, front left and front right).  $\bar{\boldsymbol{\alpha}}^f$  and  $\bar{\boldsymbol{\omega}}^f$  are the respective true values,  ${}^f\mathbf{R}_w$  is the rotation from world to the corresponding leg frame,  $\mathbf{g}$  is the gravity vector and finally  $\mathbf{b}_\alpha$ ,  $\mathbf{b}_\omega$ ,  $\mathbf{w}_\alpha$ ,

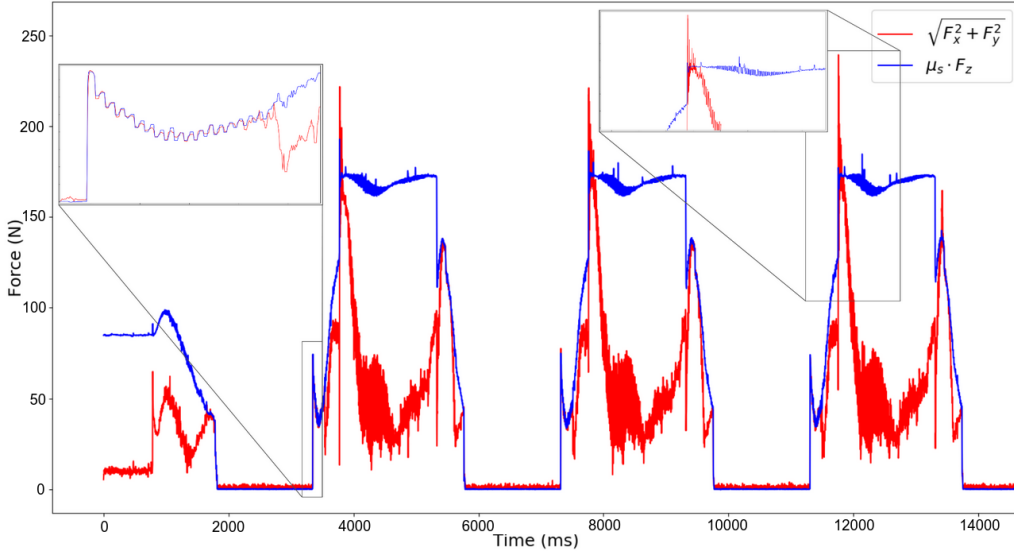


Figure 5.2: Force fluctuations during impact for the ATLAS simulated robot.

and  $w_\omega$  are the biases and the zero-mean normally distributed noises respectively. Additionally, biases and the gravity constant are removed from the accelerometer and gyroscope in real-time by estimating the rotation ( ${}^f\mathbf{R}_w$ ) with a complementary filter on the IMU measurements [52]. This simplifies the measurement model to the following:

$$\alpha^f = \bar{\alpha}^f + w_\alpha \quad (5.6)$$

$$\omega^f = \bar{\omega}^f + w_\omega \quad (5.7)$$

### 5.1.3 Complementary Filter

A complementary filter is a signal processing technique used to combine the information from multiple sensors or measurements to obtain a more accurate estimation of a desired variable or state. It effectively fuses measurements from various sensor measurements by deploying a low- and a high- pass filter. The low-pass filter allows the smooth and gradual changes in the signal to pass through, filtering out high-frequency noise or rapid fluctuations. On the other hand, the high-pass filter amplifies the high-frequency components, which are typically noise or short-term variations, and attenuates the slower changes. By appropriately adjusting the cut-off frequencies and gains of the filters, the complementary filter effectively combines the strengths of each sensor: the low-pass filter retains the long-term trend and the high-pass filter captures the short-term dynamics. This integration results in an improved estimate of the desired variable, reducing noise and eliminating the drift typically associated with individual sensors.

The complementary filter is often employed to remove biases and gravity effects from the measurements of an IMU. IMUs consist of sensors like accelerometers

and gyroscopes, which are prone to biases and gravitational influences that can degrade the accuracy of the measurements. By utilizing a complementary filter, the low-pass filtered accelerometer readings can provide an estimate of the gravity component of the sensor’s measurements, while the high-pass filtered gyroscope readings can capture the dynamic motion information. The estimated gravity component is then subtracted from the accelerometer measurements to eliminate the gravitational bias. This corrected accelerometer data is then fused with the gyroscope data to produce a more accurate representation of the IMU’s orientation or motion.

#### 5.1.4 Stable contact definition

As stated previously, at the moment of impact between the foot and the ground, and for a small period of time after that, the forces fluctuate and micro-movements of the foot occur. The same issue arises during the transition from support leg to swing. In this thesis’ scope, a contact is defined as tangentially stable when the following conditions are satisfied:

$$\bar{v}_x^f = 0 \quad (5.8)$$

$$\bar{v}_y^f = 0 \quad (5.9)$$

$$\bar{\omega}_z^f = 0 \quad (5.10)$$

where  $\bar{v}_x^f, \bar{v}_y^f$  are the true velocities of the  $f$  foot in the  $x$  and  $y$  axes, respectively. In the same manner, for the rotational stable state:

$$\bar{v}_z^f = 0 \quad (5.11)$$

$$\bar{w}_x^f = 0 \quad (5.12)$$

$$\bar{\omega}_y^f = 0 \quad (5.13)$$

As already explained in Section 5.1.1, constant velocity is infeasible in the event of breaking contact. Accordingly, Eqs. (5.8)–(5.13) can be reformulated to fit the IMU measurements as:

$$\bar{a}_x^f = \bar{a}_y^f = \bar{a}_z^f = 0 \quad (5.14)$$

$$\bar{\omega}_x^f = \bar{\omega}_y^f = \bar{\omega}_z^f = 0 \quad (5.15)$$

## 5.2 Mathematical Modeling

Assuming an ideal scenario with no uncertainties in the measurements, Eqs. (5.14) and (5.15) are sufficient to classify the contact state between the robot’s foot and the ground deterministically. However, this assumption is far from being true in real cases. In this work, we exploit the probabilistic nature of involved uncertainties to extract the stable contact probability at each time step. For the relevant

formulation we start with Eqs. (5.6) and (5.7) which can be re-written as:

$$\bar{\alpha}^f = \alpha^f - \mathbf{w}_\alpha \quad (5.16)$$

$$\bar{\omega}^f = \omega^f - \mathbf{w}_\omega \quad (5.17)$$

Since the uncertainty  $\mathbf{w}$  is modelled as a zero-mean normally distributed random variable (r.v.),  $\mathbf{w} \sim N(\mathbf{0}, \sigma^2)$ , the equations above describe the ground truth measurements as normally distributed r.v. too. In this context,  $\bar{\alpha}^f \sim N(\alpha^f, \sigma^2)$  and  $\bar{\omega}^f \sim N(\omega^f, \sigma^2)$ , where  $\alpha^f$  and  $\omega^f$  stand for the erroneous measurements from the accelerometer and gyroscope respectively. Accordingly, the goal of the proposed approach can be defined as to find the probability of the ground values to be approximately zero for all six axes.

To this end, we employ a Kernel Density Estimator (KDE) to approximate the Probability Density Function (PDF) that describes a batch of samples. In this work, the batch size has been experimentally set to 50. A good rule of thumb is to set the batch size to be an order of magnitude smaller than the sensor's refresh rate. By integrating the estimated PDF over a symmetrical interval, the stable contact probability for each axis is calculated. Finally, since the per axis probabilities are independent, the final estimate is obtained by multiplying the individual probabilities:

$$P(\text{stable} | \mathbf{m}^t, \mathbf{m}^{t-1}, \dots, \mathbf{m}^{t-d}) = \prod_{i=1}^6 P(|\mathbf{m}_i^t| < \delta_i) \quad (5.18)$$

where  $\mathbf{m} \in \mathbb{R}^6$  is the measurement vector,  $d$  is the batch size and  $\delta \in \mathbb{R}^6$  is the empirical range vector for each axis of the IMU (red lines in Fig 5.3) that indicates the interval at which the estimated PDF will be integrated. When a new measurement is acquired, we use it along with the previous ones to estimate the updated PDF. KDE is a non-parametric estimator of univariate or multivariate densities with well-defined properties [53]. The reason we employed KDE over Maximum Likelihood Estimation (MLE) to approach the PDF is to take into consideration the transition from support leg to swing, which is only possible if the PDF is multimodal.

By employing the Markov assumption and the measurement model that is presented in Section II we can formulate KDE in order to fit our case. Let  $m_1, m_2, \dots, m_n$  be independent and identically distributed IMU measurements,  $m \in \mathbb{R}^6$ . The density function is described as follows:

$$\hat{f}_h(m) = \frac{1}{nh} \sum_{i=1}^n K\left(\frac{m - m_i}{h}\right) \quad (5.19)$$

where  $\hat{f}$  is the PDF,  $n$  is the number of samples,  $h$  is termed bandwidth and  $K$  is the Gaussian kernel:

$$K(u) = \frac{1}{\sqrt{2\pi}} \exp\left(-\frac{u^2}{2}\right) \quad (5.20)$$

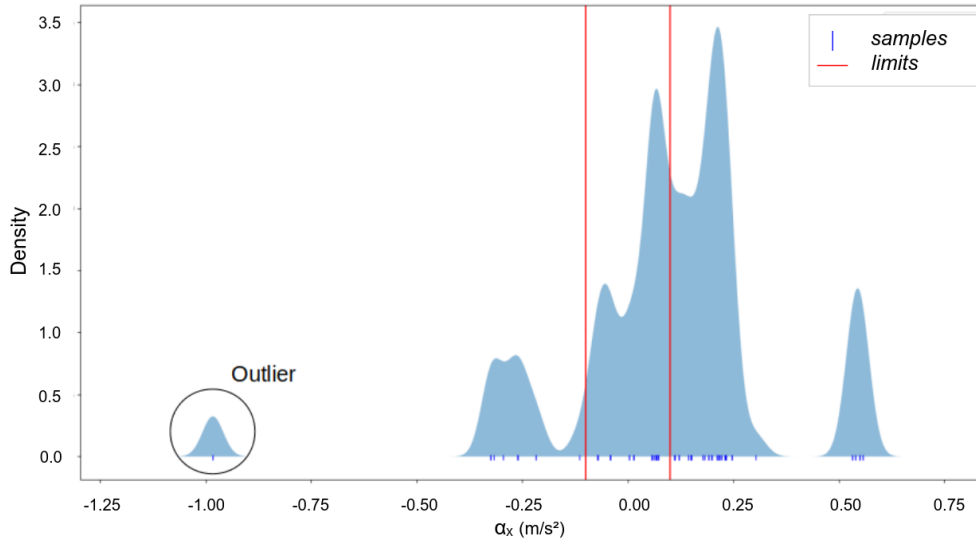


Figure 5.3: Example of estimated PDF for 100  $a_x$  samples.

The bandwidth parameter  $h$  describes how wide the PDF of every individual normally distributed sample will be represented. Naturally, we’ve chosen this parameter to be equal to the standard deviation that each sensor’s specification sheet provides. After the PDF is estimated we integrate over a small interval  $([-\delta, \delta])$  to compute the probability.

In Fig. 5.3, we present the 1-axis PDF that was estimated over a batch of 100  $a_x$  samples of the ATLAS humanoid robot in simulation. These samples are carefully selected to depict the beginning of the foot’s transition from support to swing. In any instance, that the foot is completely still and all measurements are gathered around zero, the PDF is roughly a normal distribution with mean  $\mu \approx 0$ . It is worth stating that KDE is outlier robust since few measurements do not greatly affect the overall distribution.

### 5.3 Results

The current section is dedicated to the experimental evaluation of the proposed method. Detailed testing and evaluation has been conducted by employing three different robotic platforms as well as various terrains and friction conditions. More specifically, two humanoids and one quadruped robot were used, demonstrating the generality and broad applicability of our method. For each robotic platform a number of experiments were performed which are reported and documented in the following. In addition, we have exploited the simulation environment in order to quantitatively and comparatively assess our method. In addition to the above, a more detailed illustration of our experiments is presented in high resolution at <https://youtu.be/2CEkifEAQEc>. Throughout this section, we explore the

contact state of one foot. Since each foot of the robot is identically constructed, the same process can be readily applied to the rest of the feet.

### 5.3.1 Simulation Results

The first set of experiments was conducted with a simulated ATLAS humanoid robot in a highly accurate multi-contact simulation environment namely RaiSim [43]. We generated omni-directional walking patterns by employing a stabilization module [46, 48, 49] based on Linear Inverted Pendulum (LIP) dynamics. The refresh rate of the IMU that is mounted on the sole of the robot is  $1000Hz$ . The standard deviations of the zero-mean Gaussian noises are  $\sigma_a = 0.02467 \frac{m}{s^2}$  and  $\sigma_\omega = 0.01653 \frac{rad}{s}$  for linear acceleration and angular velocity, respectively.

In the first experiment, the friction coefficient was assumed constant ( $\mu_s = 0.1$ ) and we explored the following gait pattern: Double Support (DS) and three consecutive right footsteps, i.e. Right Single Support (RSS). In Fig. 5.4 we illustrate the vertical GRF as a point of reference, the tangential stable contact probability (parallel to the walking plane), the vertical probability and finally in the same sub-figure the total predicted probability with the ground truth labels. The ground truth labels (stable/unstable) are extracted by taking into account the velocity of the sole and the vertical GRF. When the vertical GRF is greater than zero and the velocity norm of the sole is zero then the contact is classified as stable. Notice that the amplitude of the stable probability waveform for  $P_z(stable)$  is larger than the  $P_{xy}(stable)$ 's one. This occurs because the foot is stable in the vertical plane, while this is not the case for the tangential one. Since the total probability is extracted via multiplication the small probabilities of stable contact dominate the final result.

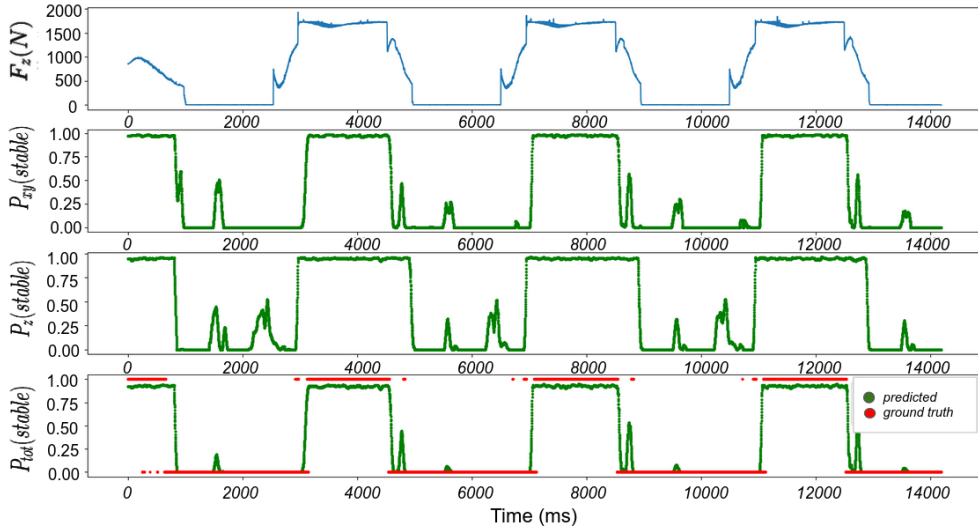


Figure 5.4: ATLAS walking on stable surface.

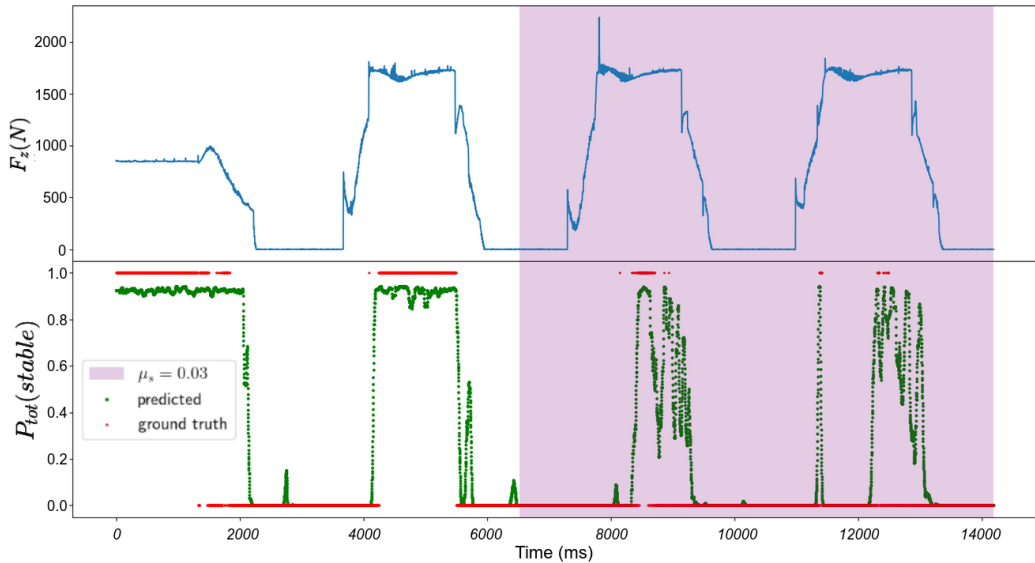


Figure 5.5: Estimated stable contact probabilities for ATLAS gaits on slippery terrain.

Next, we added a slippery surface with  $\mu_s = 0.03$  and we commanded the robot to walk over it. The robot starts at DS, then the first RSS is on a stable surface with  $\mu_s = 0.1$  while the last two are on a slippery one ( $\mu_s = 0.03$ ). In Fig. 5.5, purple region, we demonstrate the behavior of the stable contact probability when the foot is slipping. It is clear that the smooth waveform pattern from Fig. 5.4 gets disturbed in the purple region where the robot slips. Our predictions are confirmed by the ground truth labels. Note that by simply thresholding the vertical GRF, the purple region steps would be misclassified as they are identical to the first one.

### 5.3.2 Real experiments

The current section presents experimental evaluation of the proposed method with two robotic platforms, namely a TALOS humanoid and a GO1 quadruped robot. In a first experiment, the TALOS robot walked a few steps on a flat surface with sufficient friction coefficient to prevent slippage. The gait pattern is almost indistinguishable to the simulated ATLAS, since both robots are full sized humanoids with LIP-based walking pattern generation. The obtained results are presented in Fig. 5.6. As can be observed, the contact estimation probabilities follow the expected pattern which also happens to be very similar to the one observed in the case of the ATLAS robot (Fig. 5.4).

Subsequently, we evaluated extensively our method with the quadrupedal GO1 in various scenarios such as soft terrain and extremely slippery surface. In the first experiment, we commanded the robot to walk over a mattress with the default controller as provided by Unitree, to test the behavior of the contact probability

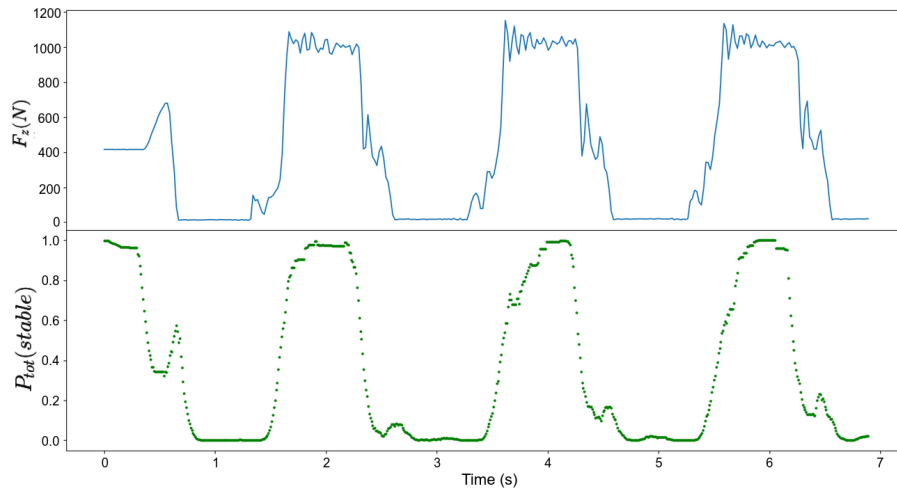


Figure 5.6: TALOS walking on a stable surface.

when the vertical GRF decreases due to low restitution. The GRF measurement was acquired from a pressure sensor mounted on the robot's end effector and was used just as a point of reference. The inertial measurements that were used for estimating the contact probability were acquired by a low-end IMU sensor (LSM6DSOX) that was manually mounted on the GO1's end effector. The purple region in Fig. 5.7 signifies the steps on the soft terrain. As verified by the bottom plot, the contact probability estimates remain unaffected by the terrain change. On the contrary, it is worth noting that approaches that utilize GRF measurements to classify the contact state would be greatly affected by the decrease of  $F_z$ .

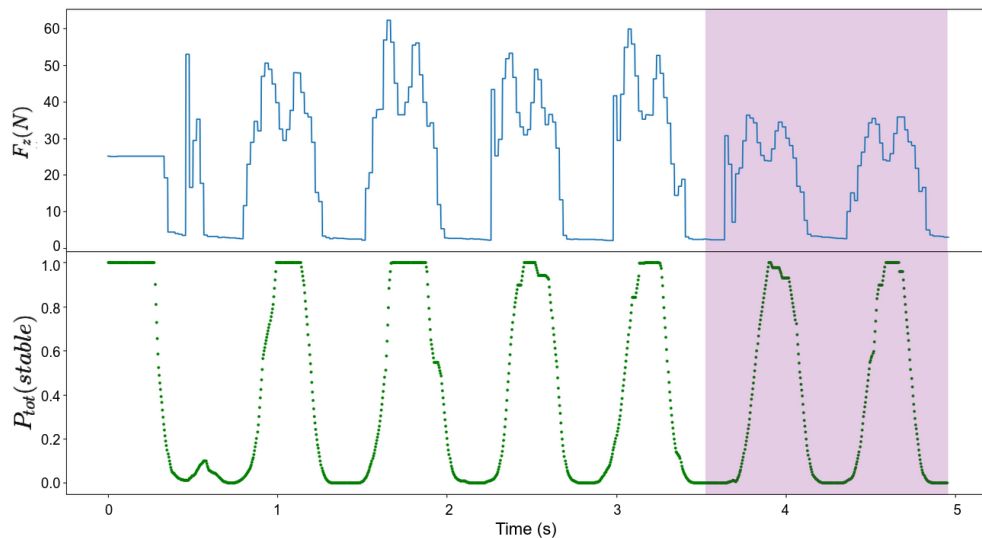


Figure 5.7: GO1 walking on soft terrain/low restitution.

For our final experiment, we greased the smooth surface that the robot was walking on to provoke extreme foot slippage. The purple region of Fig. 5.8 contains the extreme unstable steps of the robot before the grease wears out and the contacts are stable again. As Fig. 5.8 clearly shows, the contact probabilities in the greasy area are way lower indicating slippery behavior.

The proposed method can be employed in real-time with over 500 Hz refresh rate (performance measured in our implementation with a mid-range PC). We used the vertical GRF measurements to distinguish the following cases. First, when the stable probability prediction is small, the foot can be either in (a) swing phase ( $F_z = 0$ ) or (b) in unstable contact with the ground ( $F_z > 0$ ). Second, when the stable probability prediction is substantial, the foot (a) might be experiencing very small (close to zero) linear acceleration and angular velocity during swing ( $F_z = 0$ ) or (b) is in stable contact state ( $F_z > 0$ ). Nevertheless, since the vertical GRF is only considered to determine if the foot is in contact with the ground or not, an alternative would be to employ pressure or haptic sensors, even gait planning information e.g. when the leg is planned to be in swing or stance.

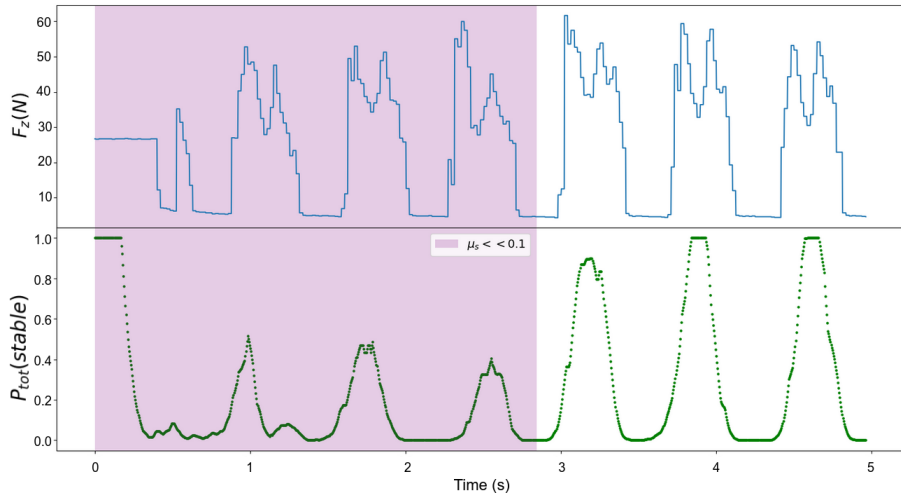


Figure 5.8: GO1 walking on slippery terrain for 3 consecutive steps.

### 5.3.3 Comparative evaluation

In order to quantitatively assess our method we have conducted comparative evaluation against a state of the art approach that probabilistically addresses the contact estimation problem [3]. Fig. 5.9 illustrates the contact probability estimations for the ATLAS simulated robot over a gaiting session that involved 22,000 discrete data points. The employed dataset is an extended version of the one previously used in Section 5.3.1. Overall, the experiment involved five footsteps with the middle three ones exhibiting highly unstable contact. Evidently, our method succeeded in correctly estimating the relevant probabilities, whereas the [3] approach

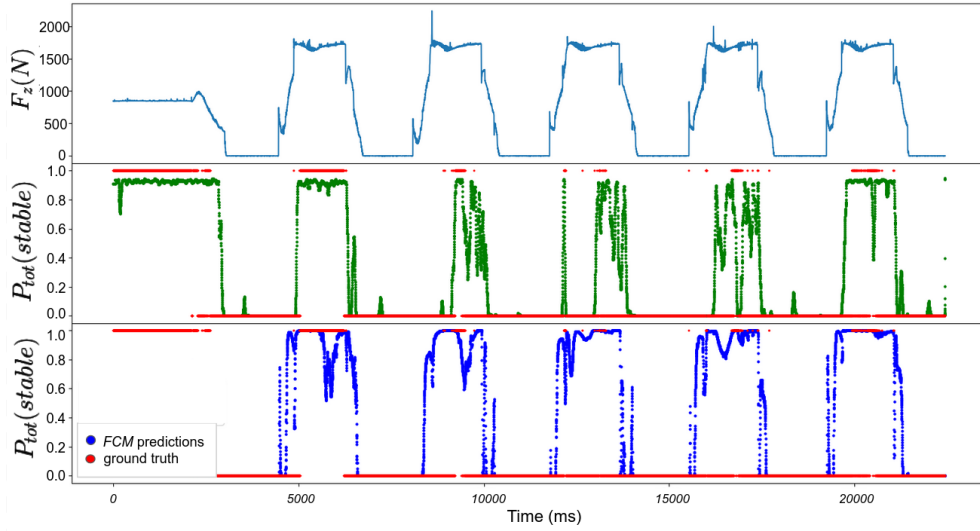


Figure 5.9: Comparative results; top row: vertical GRF; middle row: Contact probabilities as computed by proposed method; bottom row: Contact probabilities as computed by [3].

only partially accomplished the task. The latter can be interpreted by the fact that [3] depends on the full F/T measurements which undermine the estimation when the vertical GRF assumes large values. The results shown in Fig 5.9 can be compactly represented by their RMSE values, indicating superior performance for our method:

- FCM approach [3]:  $RMSE = 0.6076$
- Proposed method:  $RMSE = 0.3529$

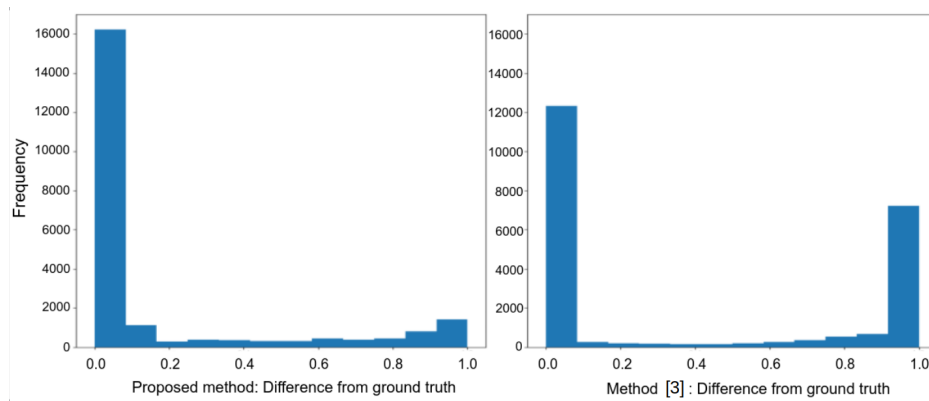


Figure 5.10: Histograms of the difference between predicted contact probability and ground truth labels.

To better appreciate the quality of the estimated contact probabilities for both approaches, Fig. 5.10 illustrates the obtained histograms of the absolute differences between ground truth and predicted probabilities. As can be observed, the number of correct predictions is significantly larger for the proposed method whereas more erroneous predictions are exhibited in [3].

In a conclusive experiment, we assessed the efficacy of this approach in a real-world slip and fall scenario using a quadruped robot. To simulate the challenging conditions, we applied a layer of grease on a flat surface and instructed the robot to traverse this terrain. Through programmed instructions, the robot was equipped with the ability to detect slippage and respond accordingly.

In the first case, when slippage was detected, the robot executed a freeze command, effectively halting its motion and preventing a potential fall. In the second case, the robot was programmed to re-initialize its posture upon slippage detection, allowing it to regain stability and continue its movement. Significantly, in both cases, the robot successfully avoided falling, showcasing the effectiveness of the active slippage detection mechanism. In contrast, when the slippage detection module was not activated, the robot faced difficulties in maintaining balance and experienced falls.

These findings underscore the critical role of slippage detection in ensuring the stability and safety of the quadruped robot in challenging terrains. The successful execution of freeze and re-initialization commands further validates the potential of this approach in mitigating slip-induced accidents and enhancing the overall performance of legged locomotion systems.

## 5.4 Conclusions

We have demonstrated that the proposed probabilistic contact estimator predicts successfully the contact state of legged robots, both in simulation and in real platforms. By employing only inertial measurements, we have shown that it can generalize in different scenarios, even in cases with extremely low static friction coefficient and successfully estimate the quality of contact. Our presentation has revealed a number of important features that are inherent in our method:

- Proprioceptive sensing is the sole information source that is employed; specifically, measurements from low-cost IMUs constitute the sensory input.
- No training data and ground truth labels are required, hence facilitating the operation of the method in practically any scenario.
- Equally important, the method is robot agnostic, making it a compelling contact estimation module for legged robots.

Overall, this approach provides a unified solution to the quality of contact detection problem, being at the same time robot and environment agnostic.



## Chapter 6

# Two-layer adaptive trajectory tracking controller for quadruped robots on slippery terrains

This chapter introduces a trajectory tracking controller (developed by peers in the Computational Vision and Robotics Laboratory), that utilizes the probabilistic contact estimation from Chapter 5, as the basis of the controller's adaptive effort distribution. This work proposes a novel trajectory tracking control scheme for quadruped robots, incorporating two prioritized layers of adaptation for minimizing possible slippage of one or multiple legs. The proposed control scheme involves two layers of adaptation, as it accounts for partially or globally slippery terrains. Both simulation and real-world experiments indicate its ability to maintain stability and controllability of the system over time. In this chapter, the controller scheme will be briefly presented while emphasising how the stable contact probability is utilized. Finally, the qualitative and quantitative results for the trajectory tracking are presented which are directly correlated with the quality and robustness of the contact estimator.

### 6.1 Problem Formulation

Consider the quadruped robot depicted in Fig. 6.1, having  $n \in \mathbb{N}$  joints in each leg and let  $q_{i,j} \in \mathbb{R}, i = 1, \dots, 4, j = 1, \dots, n$  be the joint position variables of the  $i$ -th leg. Let  $\mathbf{q} \triangleq [q_{1,1} \ q_{1,2} \ \dots \ q_{4,n-1} \ q_{4,n}]^\top \in \mathbb{R}^{4n}$  be the vector of the total joint variables of the robot. Furthermore, let  $\{C\}$  be the frame placed at the Center of Mass (CoM) of the robot (as depicted in Fig. 6.1) and  ${}^c\mathbf{p}_i(q_{i,1}, \dots, q_{i,n}) \in \mathbb{R}^3$  be the position of the tip of  $i$ -th leg with respect to  $\{C\}$ . The position and orientation of  $\{C\}$  with respect to the world frame  $\{0\}$  is denoted by  $\mathbf{p}_c \in \mathbb{R}^3$  and  $\mathbf{R}_c \in SO(3)$

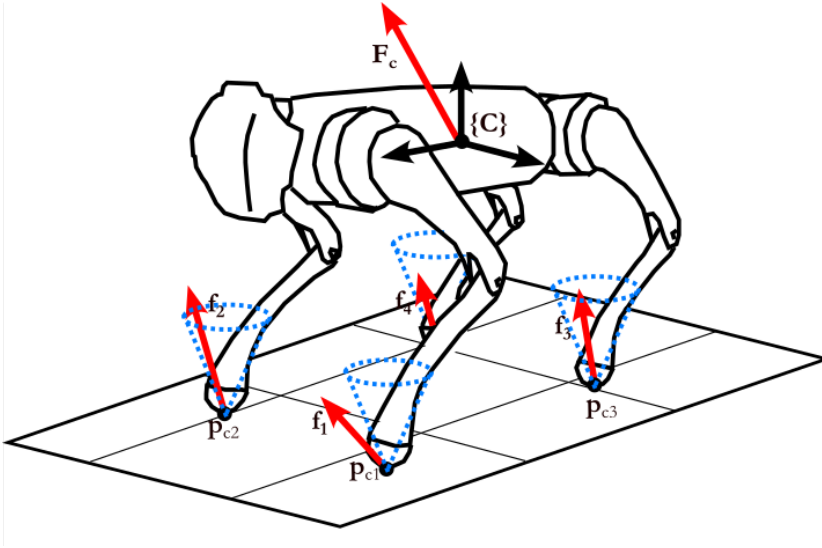


Figure 6.1: Force distribution among the legs of the quadruped robot.

respectively. World frame  $\{0\}$  could refer to a known inertial frame, or (in most of the cases) to the initial pose of the robot (i.e.  $\{C\}$  at  $t = 0$ ). When all four tips are in contact with the supporting surface, the mapping between the forces  $\mathbf{f}_i \in \mathbb{R}^3, i = 1, \dots, 4$  applied to the tips of the legs and the corresponding generalized force,  $\mathbf{F}_c \triangleq [\mathbf{f}_c^\top \boldsymbol{\tau}_c^\top]^\top \in \mathbb{R}^6$  at the CoM, with  $\mathbf{f}_c \in \mathbb{R}^3$  and  $\boldsymbol{\tau}_c \in \mathbb{R}^3$  being the force and torque at the CoM respectively, is the following:

$$\mathbf{F}_c = \mathbf{G}(\mathbf{q})\mathbf{F}_a, \quad (6.1)$$

where

$$\mathbf{G}(\mathbf{q}) \triangleq \begin{bmatrix} \mathbf{I}_3 & \mathbf{I}_3 & \mathbf{I}_3 & \mathbf{I}_3 \\ \mathbf{S}(\mathbf{p}_{c1}) & \mathbf{S}(\mathbf{p}_{c2}) & \mathbf{S}(\mathbf{p}_{c3}) & \mathbf{S}(\mathbf{p}_{c4}) \end{bmatrix} \quad (6.2)$$

and

$$\mathbf{F}_a \triangleq \begin{bmatrix} \mathbf{f}_1 \\ \mathbf{f}_2 \\ \mathbf{f}_3 \\ \mathbf{f}_4 \end{bmatrix} \in \mathbb{R}^{12}, \quad (6.3)$$

with  $\mathbf{p}_{ci}(q_{i,1}, \dots, q_{i,n}) \triangleq \mathbf{R}_c^c \mathbf{p}_i(q_{i,1}, \dots, q_{i,n}), i = 1, \dots, 4$ ,  $\mathbf{I}_3 \in \mathbb{R}^{3 \times 3}$  the identity matrix and  $\mathbf{S}(\cdot) : \mathbb{R}^3 \rightarrow \mathbb{R}^{3 \times 3}$  the skew symmetric mapping. Notice that  $\mathbf{G}(\mathbf{q})$  belongs to  $\mathbb{R}^{6 \times 12}$ , and therefore the problem of solving (6.1) with respect to  $\mathbf{F}_a$ , i.e. finding  $\mathbf{F}_a$  for a given  $\mathbf{F}_c$ , is redundant.

Based on the given system representation, our objective is to determine the appropriate forces to apply at the center of mass (CoM) in order to keep the forces at the tip of each leg within the boundaries of the friction cone. The friction cone is defined by Equation 5.3, and when the force remains within this cone, the contact is considered stable. Since the exact value of the static friction coefficient

is unknown, we implement measures to address slippage and maintain control over the system, while ensuring uninterrupted progress towards the desired task.

## 6.2 Proposed Scheme

Building on the probabilistic contact estimator as formulated in Chapter 5, a novel trajectory tracking control scheme incorporating a two-layer on-line adaptation is proposed. In particular, the probability of a contact being stable is estimated in real-time, based on a set of IMU sensors mounted on the robot’s feet. This probability is counter proportional to the probability of slippage. Based on this estimate, we firstly propose an adaptation law for the weights of distribution of the control effort among all the directions of forces that should be applied by each leg of the robot. The rationale behind the adaptation law is to append less tangential to the surface forces to the legs for which the slippage probability is high, attracting in this way the appended force towards the friction cone. Furthermore, when the aforementioned force distribution cannot guarantee the elimination of slippage, we propose the dynamic time-scaling of the trajectory (e.g. to slow down the motion), which will consequently yield a reduced control effort magnitude in general.

### 6.2.1 First layer of adaptation: Adaptive effort distribution

Based on the above, we propose the following adaptive law for the weights  $w_{i,m}$ ,  $m = 1, 2$  (the  $x - y$  coefficients) of the tangential force directions of the  $i$ -th leg:

$$\boxed{\dot{w}_{i,1} = \dot{w}_{i,2} \triangleq \alpha P_i}, \quad (6.4)$$

$$w_{i,1}(0) = w_{i,2}(0) \triangleq w_0$$

where  $\alpha \in \mathbb{R}^+$  is a tunable constant adaptation gain,  $w_0 \in \mathbb{R}^+$  the initial value of the weights in  $x - y$  direction and  $P_i \in [0, 1]$  the probability of slippage of the  $i$ -th leg.

Given (6.4), the weights will increase only as long as slippage is estimated, which means that the weights will eventually reach the value in which the control effort appended to the specific leg does not yield any slippage. The increase of these weights (i.e. the weights corresponding only to the tangential forces) will result in decreasing the magnitude of forces appended towards these directions. Therefore, the appended force  $\mathbf{f}_i$  will converge to the friction cone  $\mathcal{C}$ , as graphically depicted in Fig.6.2.

### 6.2.2 Second layer of adaptation: Trajectory time-scaling

The first layer of adaptation could fail when all the legs of the robot are contacting a terrain with a relatively low static friction coefficient. Hence, to handle this type of occasions, we propose the time-scaling of the trajectory, i.e. to sacrifice

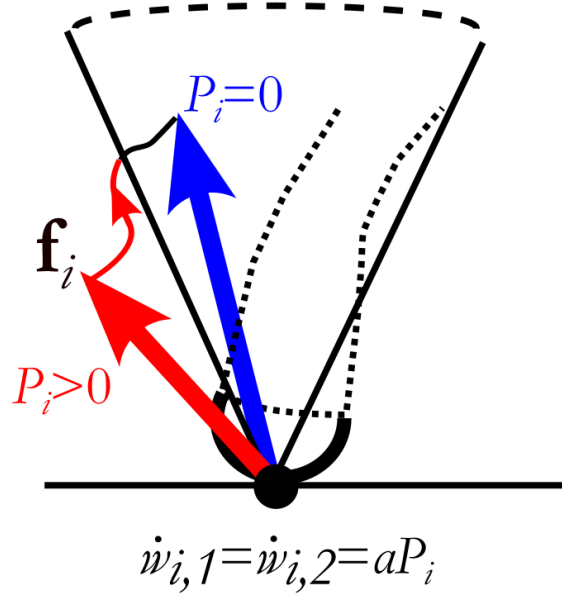


Figure 6.2: Convergence of the control effort of each leg towards the friction cone.

the temporal accuracy of the task for guaranteeing stability and controllability, maintaining however accuracy with respect to the spatial properties of the path.

To incorporate the trajectory time scaling layer, we must initially establish a parameter that quantifies the extent of this scaling. So, in order to tackle the problem of global slippage, we propose the utilization of the following time-scaling coefficient:

$$\beta(t) \triangleq \frac{w_0}{\min(w_{1,1}, w_{2,1}, w_{3,1}, w_{4,1})}. \quad (6.5)$$

The evolution of the scaled time parameter is characterized by  $\dot{t}_v(t) = \beta(t)$ . For instance, setting a constant  $\beta = 1$  would result in  $t_v = t$  and consequently would lead to the execution of the trajectory on a nominal speed, while setting  $\beta < 1$  would slow down the motion. The core idea behind (6.5) is to reduce the speed (reflected by  $\beta$ ) when slippage has occurred in all four legs, an occasion which is signified by the increase of the weights of all four legs due to (6.4). For instance, if at least one of the legs does not face any slippage, then  $\min(w_{1,1}(t), w_{2,1}(t), w_{3,1}(t), w_{4,1}(t))$  will be equal to  $w_0$  and therefore  $\beta$  will be 1, which means that no time scaling would occur.

## 6.3 Simulation study

To assess the performance of the proposed adaptive control scheme we consider three simulation scenarios: a) A simple point-to-point motion to evaluate the trajectory tracking performance, b) a scenario involving the tracking of a periodic motion with the rear right foot contacting a slippery surface and c) a scenario involving the tracking of a periodic motion with global slippage, i.e. all four legs are contacting a slippery surface. For the simulations, the model of a Unitree Go1 robot is utilized in the Gazebo environment and a control cycle of 2ms is considered. In Fig. 6.3 the simulation environment is shown, with the yellow area representing the slippery terrain considered in the second scenario (slippage of the rear right foot).

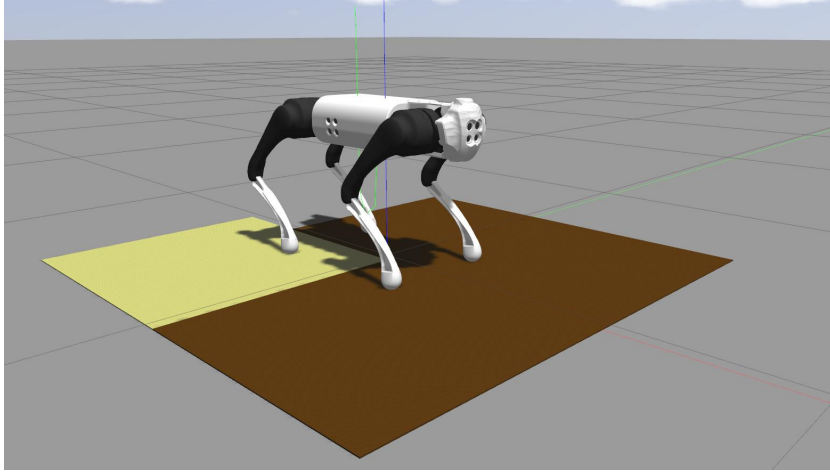


Figure 6.3: The initial configuration of the simulations. Yellow area: The slippery area considered for the second scenario.

### 6.3.1 Scenario 1: Point to point motion

For this scenario, a terrain with a static friction coefficient of 1.4 is considered, representing a non-slippery terrain. The desired trajectory is generated online by the following first order dynamical system:  $\dot{\mathbf{p}}_d(t) = \mathbf{p}_d(t) - \mathbf{p}_T$ , with  $\mathbf{p}_T = \mathbf{p}_d(0) + [0.1 \ 0.05 \ -0.005]^\top$  being the constant target. The initial actual and desired values are  $\mathbf{p}(0) = [-0.043 \ -0.0037 \ 0.356]^\top \text{m}$  and  $\mathbf{p}_d(0) = [-0.023 \ 0.0063 \ 0.355]^\top \text{m}$  in order to impose an initial position error of  $\mathbf{e}_p = [-2 \ -1 \ 0.1]^\top \text{cm}$ . In Fig. 6.4 the actual position evolution is compared to the desired trajectory, in which one can notice the tracking performance. Notice that the tracking performance is affected by the unmodelled joint friction that acts as a disturbance to the system, with the  $z$ -direction being the most disturbed direction, due to the manipulability ellipsoid of the given robot's configuration. One could possibly reduce this steady state

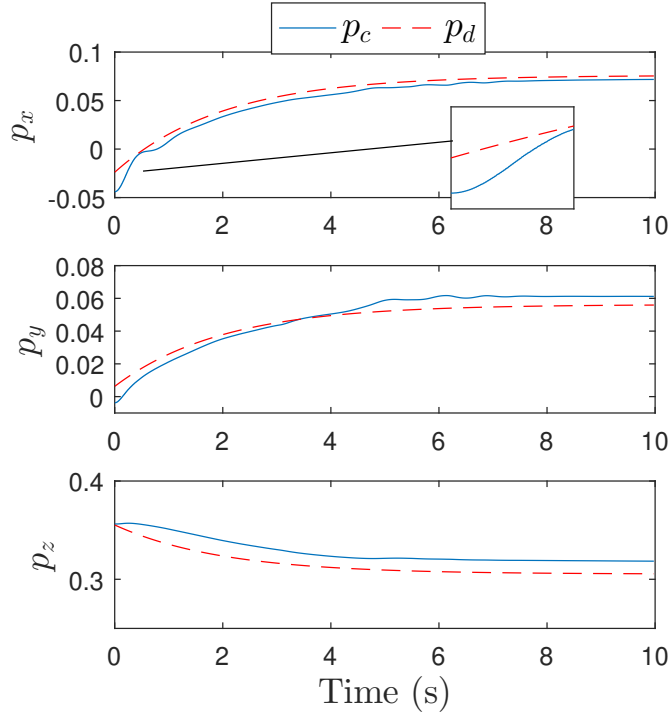


Figure 6.4: [Scenario 1: Point-to-point motion] Time evolution of the actual and desired position.

error by further tuning the control gains (as no extensive tuning was performed), or by incorporating an additional integral term to the controller.

### 6.3.2 Scenario 2: One-foot slippage

For the second scenario, the rear right foot of the robot ( $i = 3$ ) is considered to contact a slippery surface having a static friction coefficient of 0.4, which is considered to be unknown for the controller. For the rest of the feet a non-slippery surface is considered. For comparison, two tests are performed, namely one with the adaptive mechanism and the other without it. The desired trajectory involves a periodic sinusoidal motion, executing an ellipse on the  $x - z$  plane, for position and a periodic rotation around the  $x$ -axis for orientation. The weights of distribution along the  $x$  direction of each leg (which is equal to the ones along the  $y$  direction), i.e.  $w_{i,1}$ , are depicted in Fig. 6.5, alongside with the stable contact probability provided by the estimator, i.e.  $1 - P_i$ . Notice the rise of the value of  $w_{3,1}$  (the leg that slips), which results in appending less force along the  $x - y$  directions of the third leg. Further notice that the third leg stops slipping after the adaptation which means that the force converged to a value within the friction cone and the system reaches a stable steady-state condition. In Fig. 6.6, the position and orientation errors are depicted, with and without the proposed adaptive scheme for

comparison purposes. Notice that without the proposed adaptation mechanism, the system is not able to maintain its stability, as the robot loses contact with the environment at  $t \approx 4.5$ s. Last, notice that  $\beta = 1$  during the whole simulation, due to equation (6.5) and the fact that  $w_{i,1} = 35, \forall i = 1, 2, 4$ , which means that the first adaptation layer can sufficiently provide a solution by dynamically distributing the control effort.

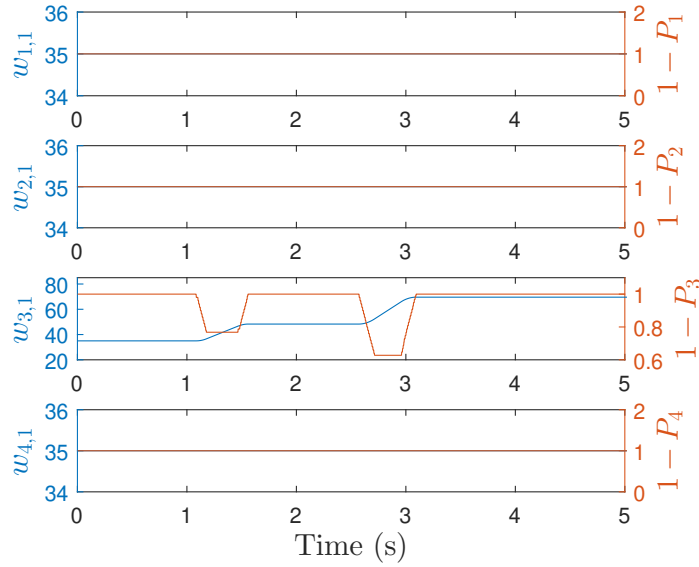


Figure 6.5: [Scenario 2: One-foot slippage] Weight adaptation due to the first layer (the second layer is not enabled).

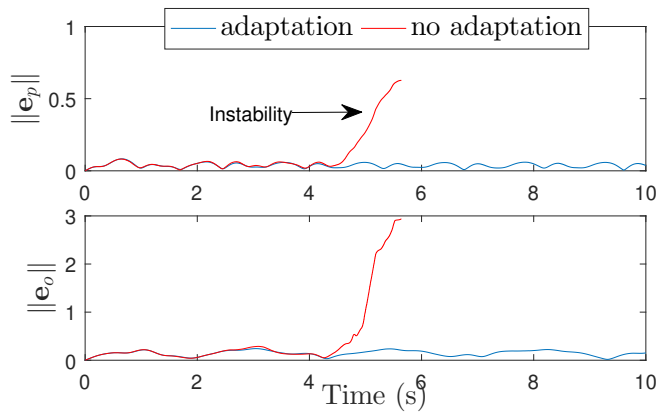


Figure 6.6: [Scenario 2: One-foot slippage] Position and orientation error norms with and without adaptation.

### 6.3.3 Scenario 3: Global slippage

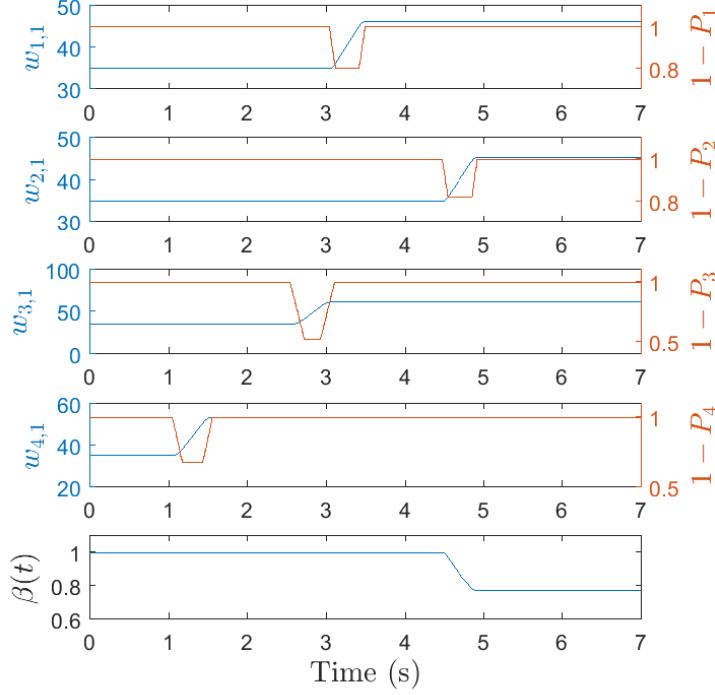


Figure 6.7: [Scenario 3: Global slippage] Weight adaptation due to the first and second layer.

For this scenario, all four legs of the robot are considered to contact the slippery surface having a static friction coefficient of 0.4. For comparison, we performed two tests, namely one with the adaptive control scheme and one without it and the same trajectory with that of the second scenario is considered. The weights of distribution along the  $x$  direction of each leg (which is equal to the ones along the  $y$  direction), i.e.  $w_{i,1}$ , as well as the time-scaling parameter  $\beta(t)$  are depicted in Fig. 6.7, alongside with the stable contact probability provided from the estimator. Notice the rise of the values of all  $w_{i,1}$ ,  $i = 1, \dots, 4$ , which results in slowing down the motion, which is reflected by the reduction of  $\beta(t)$  which converges to the value of  $\beta \approx 0.77$  after  $t \approx 5$ s.

In Fig. 6.8, the evolution of the position of the CoM in time is depicted both with and without the proposed control scheme. Notice that without the proposed adaptation mechanism, the system is, also in this case, not able to maintain the stability of the system as the robot, signified by the drop of the CoM. Last, notice the smooth on-line time-scaling of the trajectory occurred after  $t \approx 5$ s.

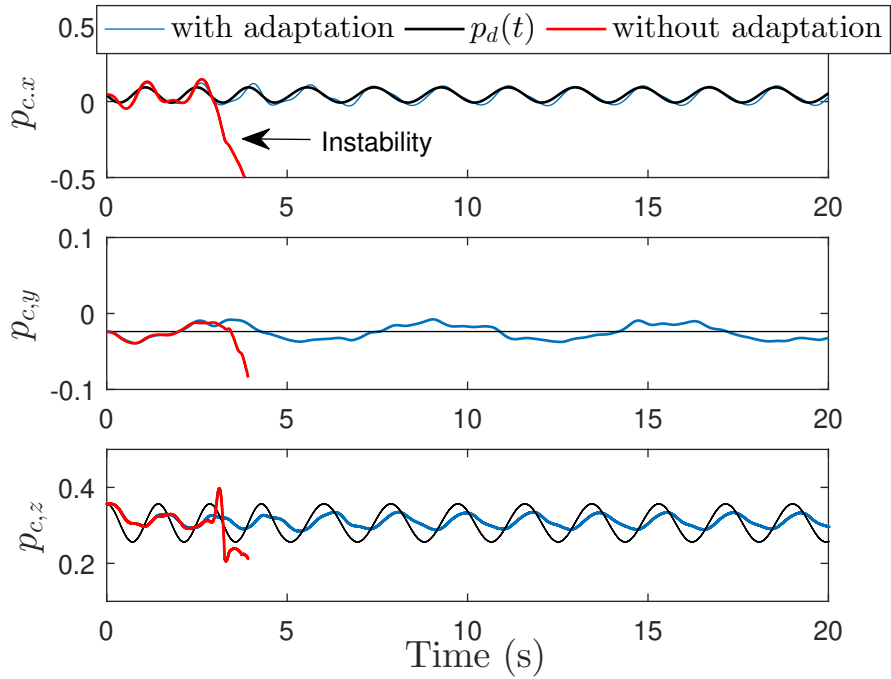


Figure 6.8: [Scenario 3: Global slippage] Evolution of the position of the CoM in time, with and without adaptation.

## 6.4 Experimental validation

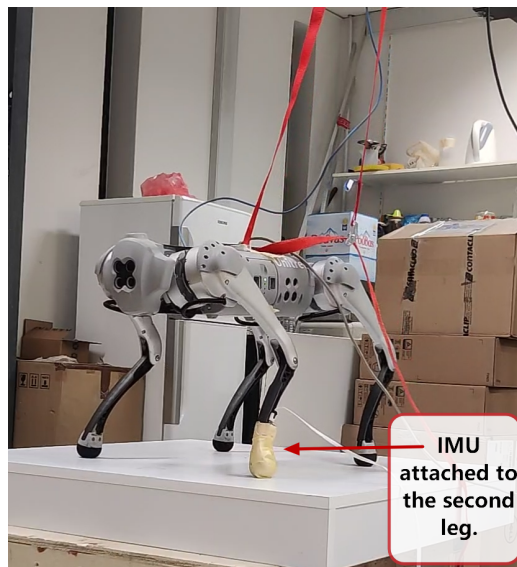


Figure 6.9: The experimental setup and initial configuration of the robot.

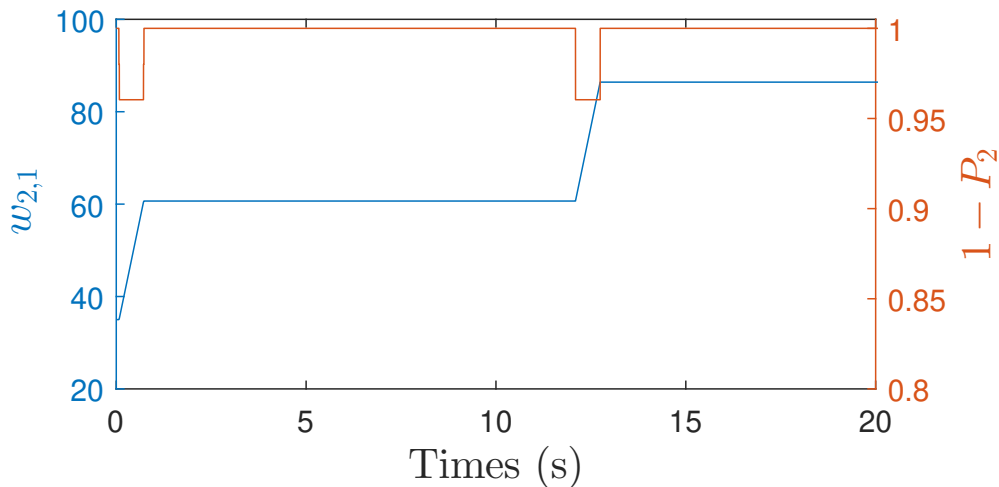


Figure 6.10: The second weight during the experimental validation.

The real world experimental validation is performed on a Unitree Go1 robot, to validate the adaptation performed by the first layer of the adaptation mechanism. In particular, a 6DOF IMU is attached to the second leg of the robot, as shown in Fig. 6.9, which is in contact with a slippery surface, (i.e. lubricant is utilized to emulate the slippery area below the second leg), while the pose of the robot is found on-line via an external camera with an off-the-shelf visual odometry system and therefore initial robot's pose is considered as the world frame for the experiment. The robot was commanded to move along the  $x$ -axis with a similar to the second simulation periodic trajectory for the axis of motion, having a frequency of 0.4Hz. In Fig. 6.10, the weight corresponding to the  $x - y$  directions of the second leg is given, alongside with the slippage probability estimate; the weights of the rest of the legs remained unaltered during the experiment. In Fig.6.11 the evolution of position in time is depicted utilizing the adaptive scheme and without its utilization, for comparison. Notice that the activation of the first adaptation layer results in maintaining stability, while when executing the same scenario without enabling the adaptation mechanism the robot is not able to maintain stability at  $t \approx 14.6$ s. Further, notice that without the adaptation mechanism the tracking performance is affected by the slippage of the second leg, as it triggers unmodelled dynamics.

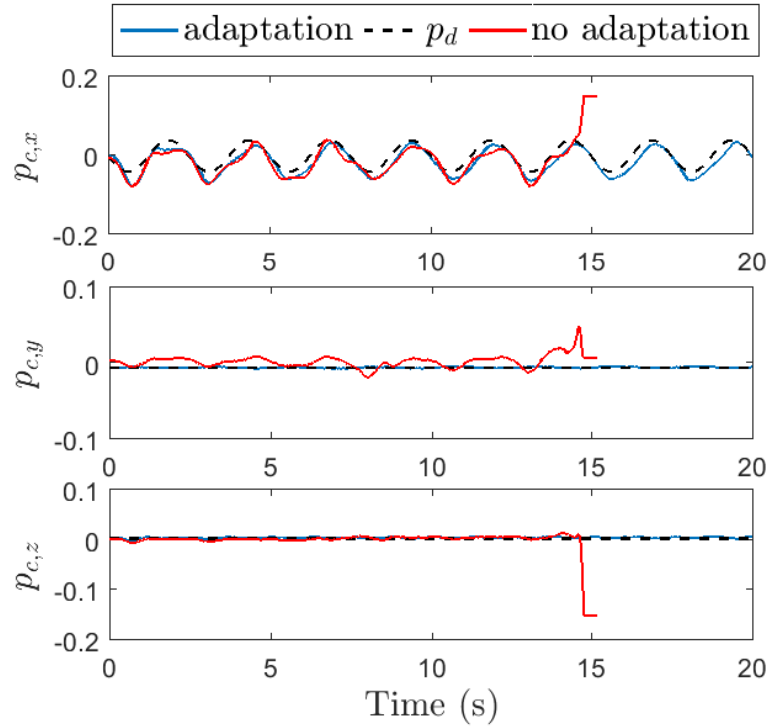


Figure 6.11: Evolution of the position of the CoM in time, with and without adaptation.

## 6.5 Conclusions

In this chapter, an adaptive trajectory tracking controller is presented for quadruped robots, which involves two prioritized layers of adaptation for minimizing the slippage of one or multiple legs. The first adaptation layer considers the dynamic distribution of the control effort among the legs, given the slippage probability for each leg. The second layer, which is enabled only if the problem cannot be solved by the dynamic distribution of the effort, which may occur when all four legs slip, acts on the time-scaling of the trajectory by dynamically and smoothly slowing down the motion, without affecting the spatial properties of the task. The proposed method is proven to be asymptotically stable. Furthermore, it is shown through simulations and experiments that the method equips the system with robustness, as it is able to minimize the slippage of the legs and it ensures the stability and controllability of the robot. Finally, the real-time weight adaptation which results in robust trajectory tracking, indicates the robustness of the model-based probabilistic contact estimation module which can accurately predict the slippage probability in real-time.



# Chapter 7

## Conclusions

### 7.1 Summary

This thesis explores the challenges associated with contact estimation for legged robots, aiming to address these challenges by proposing two novel approaches. Deploying legged robots in real-world environments poses a significant and intricate challenge due to the unpredictable and harsh conditions they inevitably encounter. To effectively and reliably operate in real-world scenarios, improvements are required in enhancing the resilience, stability, and efficiency of legged locomotion in unstructured and dynamic environments. This research pushed the limits of existing approaches in the relevant field and contributed to advancing the capabilities of legged robots.

One of the proposed approaches is a supervised deep learning framework, coined as LCD, designed specifically to achieve accurate and robust contact detection in bipedal robots. LCD leverages the strengths of proprioceptive sensing, incorporating F/T and IMU measurements, to predict the quality of contact. By analyzing the data from these sensors, LCD can successfully estimate the contact state and provide valuable insight into the stability and reliability of the robot's interactions with the environment. The main advantage of LCD is its ability to generalize across different robotic platforms, making it applicable to various bipedal robots. Furthermore, LCD demonstrates a seamless transition from simulation to real-world setups, contributing to its practicality and applicability in real-world deployment scenarios. Experimental validation conducted in both simulated and real environments confirms the effectiveness of LCD in accurately estimating the contact state and assessing the quality of contact. However, it should be noted that the utilization of LCD requires training data with appropriate noise modeling and ground truth labels, which are typically obtained from simulation environments. This reliance on simulated data is a limitation that should be considered for practical implementation.

To this end, another approach is presented in this thesis, focusing on contact estimation solely through inertial measurements. This approach offers a promising

alternative that can be deployed for legged robots with different configurations without the need for prior training. By utilizing IMU sensors mounted on each end-effector of the robot, this method successfully predicts the contact state in both simulated and real-world scenarios. The exclusivity of inertial measurements as the information source provides notable advantages, including generalizability across different scenarios, even in cases involving extremely low static friction coefficients. The reliance on low-cost IMUs as the primary sensing modality eliminates the need for extensive training data and ground truth labels, making this approach more practical and accessible for real-world implementation.

In conclusion, to further evaluate and validate the model-based approach, an adaptive trajectory tracking controller is presented, leveraging the contact probability to adapt the joint weights. The adaptive nature of this controller, which relies on accurate contact state estimation, enhances the overall robustness and performance of the legged robot. By effectively utilizing the estimated contact state, the controller can dynamically adjust the joint weights to achieve optimal stability and controllability. This integration of contact estimation with the trajectory tracking controller demonstrates the critical role of accurate contact state information in achieving robust locomotion.

## 7.2 Future Work

In our future work, we plan to develop a base state estimation framework for legged robots while considering the contact state in every update step. This is typically accomplished through slip rejection, where kinematics measurements are discarded when the robot experiences slipping. However, our objective is to delve deeper into the phenomenon of slippage and utilize these measurements in the update step, rather than rejecting them. There are various possible approaches to accomplish this objective. One approach involves estimating both the direction and velocity of slippage and incorporating these variables into the update step. By accurately determining the direction and velocity of slippage, the controller can adjust the robot's actions and generate appropriate forces to counteract and prevent further slippage in subsequent steps. This estimation of slippage parameters adds valuable information to the control loop, enabling the controller to make informed decisions and adapt its actions accordingly.

Additionally, another potential state variable that can be incorporated into the system is an estimation of the static friction coefficient. By estimating this coefficient, the controller gains insight into the surface characteristics and can generate the necessary forces to ensure sufficient traction and prevent slippage. The accurate estimation of the static friction coefficient allows the controller to optimize its actions based on the specific surface conditions and dynamically adjust the generated forces to maintain stable and non-slip motion.

Moreover, our plan entails the development of a dynamic locomotion scheme that can adapt in real-time based on the aforementioned state estimate. The goal

is to achieve robust and agile locomotion across various terrains. Unlike existing controllers that often freeze or halt in the presence of slippage, our locomotion scheme has the potential to effectively address slip detection to prevent falls and mitigate potential damage to the robot's hardware. This approach aims to avoid catastrophic events and enhance the overall capabilities and functionality of legged robots in real-world applications.

In summary, our future work focuses on a novel perspective of slippage detection, utilizing the measurements rather than discarding them, and aims to create a dynamic locomotion scheme that can adapt and excel in challenging terrains. By doing so, we aim to significantly enhance the capabilities of legged robots, enabling them to operate more effectively and safely in real-world scenarios.



# Bibliography

- [1] M. F. Fallon, M. Antone, N. Roy, and S. Teller. Drift-free Humanoid State Estimation Fusing Kinematic, Inertial and LIDAR Sensing. In *IEEE-RAS Intl. Conf. on Humanoid Robots*, pages 112–119, 2014.
- [2] Stephane Caron. Robotics lectures. <https://scaron.info/robotics/equations-of-motion.html>.
- [3] N. Rotella, S. Schaal, and L. Righetti. Unsupervised Contact Learning for Humanoid Estimation and Control. In *Proceedings of the IEEE International Conference on Robotics and Automation (ICRA)*, 2018.
- [4] Ali Zamani, Mahdi Khorram, and S. Ali A. Moosavian. Dynamics and stable gait planning of a quadruped robot. In *2011 11th International Conference on Control, Automation and Systems*, pages 25–30, 2011.
- [5] Takahiro Miki, Joonho Lee, Jemin Hwangbo, Lorenz Wellhausen, Vladlen Koltun, and Marco Hutter. Learning robust perceptive locomotion for quadrupedal robots in the wild. *Science Robotics*, 7(62):eabk2822, 2022.
- [6] Shaohang Xu, Lijun Zhu, and Chin Pang Ho. Learning efficient and robust multi-modal quadruped locomotion: A hierarchical approach. In *2022 International Conference on Robotics and Automation (ICRA)*, pages 4649–4655, 2022.
- [7] Christian Gehring, Stelian Coros, Marco Hutter, Carmine Dario Bellicoso, Huub Heijnen, Remo Diethelm, Michael Bloesch, Peter Fankhauser, Jemin Hwangbo, Mark Hoepflinger, and Roland Siegwart. Practice makes perfect: An optimization-based approach to controlling agile motions for a quadruped robot. *IEEE Robotics and Automation Magazine*, 23(1):34–43, 2016.
- [8] Stylianos Piperakis, Maria Koskinopoulou, and Panos Trahanias. Nonlinear state estimation for humanoid robot walking. *IEEE Robotics and Automation Letters*, 3(4):3347–3354, 2018.
- [9] Nicholas Rotella, Michael Bloesch, Ludovic Righetti, and Stefan Schaal. State estimation for a humanoid robot. In *2014 IEEE/RSJ International Conference on Intelligent Robots and Systems*, pages 952–958, 2014.

- [10] Marco Camurri, Milad Ramezani, Simona Nobili, and Maurice Fallon. Pronto: A multi-sensor state estimator for legged robots in real-world scenarios. *Frontiers in Robotics and AI*, 7, 2020.
- [11] Fabian Jenelten, Takahiro Miki, Aravind E Vijayan, Marko Bjelonic, and Marco Hutter. Perceptive locomotion in rough terrain – online foothold optimization. *IEEE Robotics and Automation Letters*, 5(4):5370–5376, 2020.
- [12] Fabian Jenelten, Ruben Grandia, Farbod Farshidian, and Marco Hutter. Tamols: Terrain-aware motion optimization for legged systems. *IEEE Transactions on Robotics*, PP:1–19, 12 2022.
- [13] Péter Fankhauser, Michael Bloesch, and Marco Hutter. Probabilistic terrain mapping for mobile robots with uncertain localization. *IEEE Robotics and Automation Letters*, 3(4):3019–3026, 2018.
- [14] Emmanouil Hourdakakis, Stylianos Piperakis, and Panos Trahanias. roboslam: Dense rgb-d slam for humanoid robots. In *2021 IEEE/RSJ International Conference on Intelligent Robots and Systems (IROS)*, pages 2224–2231, 2021.
- [15] M. Maravgakis, Despina-Ekaterini Argiropoulos, S. Piperakis, and P. Trahanias. Probabilistic contact state estimation for legged robots using inertial information. In *IEEE International Conference on Robotics and Automation* <https://arxiv.org/abs/2303.00538>, 2023.
- [16] Stylianos Piperakis, Michael Maravgakis, Dimitrios Kanoulas, and Panos Trahanias. Robust contact state estimation in humanoid walking gaits. In *2022 IEEE/RSJ International Conference on Intelligent Robots and Systems (IROS)*, pages 6732–6738, 2022.
- [17] Twan Koolen, Sylvain Bertrand, Gray Thomas, Tomas de Boer, Tingfan Wu, Jesper Smith, Johannes Engelsberger, and Jerry Pratt. Design of a momentum-based control framework and application to the humanoid robot atlas. *Intl. Journal of Humanoid Robotics*, 13:1650007, 2016.
- [18] Alexander Herzog, Nicholas Rotella, Sean Mason, Felix Grimmering, Stefan Schaal, and Ludovic Righetti. Momentum control with hierarchical inverse dynamics on a torque-controlled humanoid. *Auton. Robots*, 40(3):473–491, March 2016.
- [19] M. Neunert, M. Stäuble, M. Gifftthaler, C. D. Bellicoso, J. Carius, C. Gehring, M. Hutter, and J. Buchli. Whole-body nonlinear model predictive control through contacts for quadrupeds. *IEEE Robotics and Automation Letters*, 3(3):1458–1465, July 2018.
- [20] B. Aceituno-Cabezas, C. Mastalli, H. Dai, M. Focchi, A. Radulescu, D. G. Caldwell, J. Cappelletto, J. C. Grieco, G. Fernández-López, and C. Semini. Simultaneous contact, gait, and motion planning for robust multilegged

- locomotion via mixed-integer convex optimization. *IEEE Robotics and Automation Letters*, 3(3):2531–2538, 2018.
- [21] A. W. Winkler, C. D. Bellicoso, M. Hutter, and J. Buchli. Gait and trajectory optimization for legged systems through phase-based end-effector parameterization. *IEEE Robotics and Automation Letters*, 3(3):1560–1567, July 2018.
- [22] Ayonga Hereid, Christian M Hubicki, Eric A Cousineau, and Aaron D Ames. Dynamic Humanoid Locomotion: A Scalable Formulation for HZD Gait Optimization. *IEEE Transactions on Robotics*, 2018.
- [23] Nicholas Rotella, Michael Bloesch, Ludovic Righetti, and Stefan Schaal. State estimation for a humanoid robot. In *2014 IEEE/RSJ International Conference on Intelligent Robots and Systems*, pages 952–958, 2014.
- [24] Michael Bloesch, Marco Hutter, MH Hoepflinger, Stefan Leutenegger, Christian Gehring, C David Remy, and Roland Siegwart. State Estimation for Legged Robots—Consistent Fusion of Leg Kinematics and IMU . *Robotics Sci. and Sys.*, 2012.
- [25] Vignesh Sushrutha Raghavan, Dimitrios Kanoulas, Chengxu Zhou, Darwin G. Caldwell, and Nikos G. Tsagarakis. A Study on Low-Drift State Estimation for Humanoid Locomotion, Using LiDAR and Kinematic-Inertial Data Fusion. In *IEEE-RAS 18th International Conference on Humanoid Robots (Humanoids)*, pages 1–8, 2018.
- [26] S. Piperakis, D. Kanoulas, N. G. Tsagarakis, and P. Trahanias. Outlier-robust state estimation for humanoid robots. In *2019 IEEE/RSJ International Conference on Intelligent Robots and Systems (IROS)*, pages 706–713, 2019.
- [27] N. Rotella, A. Herzog, S. Schaal, and L. Righetti. Humanoid momentum estimation using sensed contact wrenches. In *IEEE-RAS Intl. Conf. on Humanoid Robots*, pages 556–63, 2015.
- [28] S. Piperakis and P. Trahanias. Non-linear ZMP based State Estimation for Humanoid Robot Locomotion. In *IEEE-RAS Intl. Conf. on Humanoid Robots*, pages 202–209, 2016.
- [29] S. Piperakis, M. Koskinopoulou, and P. Trahanias. Nonlinear State Estimation for Humanoid Robot Walking. *IEEE Robotics and Automation Letters*, 3(4):3347–3354, Oct 2018.
- [30] Michael Bloesch, Marco Hutter, Mark Hoepflinger, Stefan Leutenegger, Christian Gehring, C. David Remy, and Roland Siegwart. State estimation for legged robots - consistent fusion of leg kinematics and IMU. In *Proceedings of Robotics: Science and Systems*, Sydney, Australia, July 2012.

- [31] Michael Bloesch, Christian Gehring, Péter Fankhauser, Marco Hutter, Mark A. Hoepflinger, and Roland Siegwart. State estimation for legged robots on unstable and slippery terrain. In *2013 IEEE/RSJ International Conference on Intelligent Robots and Systems*, pages 6058–6064, 2013.
- [32] Gerardo Bleedt, Patrick M. Wensing, Sam Ingersoll, and Sangbae Kim. Contact model fusion for event-based locomotion in unstructured terrains. In *2018 IEEE International Conference on Robotics and Automation (ICRA)*, pages 4399–4406, 2018.
- [33] Jemin Hwangbo, Carmine Dario Bellicoso, Péter Fankhauser, and Marco Hutter. Probabilistic foot contact estimation by fusing information from dynamics and differential/forward kinematics. In *2016 IEEE/RSJ International Conference on Intelligent Robots and Systems (IROS)*, pages 3872–3878, 2016.
- [34] Scott Kuindersma, Robin Deits, Maurice Fallon, Andrés Valenzuela, Hongkai Dai, Frank Permenter, Twan Koolen, Pat Marion, and Russ Tedrake. Optimization-based locomotion planning, estimation, and control design for the atlas humanoid robot. *Autonomous Robots*, 40, 07 2015.
- [35] Michael Neunert, Farbod Farshidian, Alexander W. Winkler, and Jonas Buchli. Trajectory optimization through contacts and automatic gait discovery for quadrupeds. *IEEE Robotics and Automation Letters*, 2:1502–1509, 2016.
- [36] Michele Focchi, Victor Barasuol, Marco Frigerio, Darwin G. Caldwell, and Claudio Semini. *Slip Detection and Recovery for Quadruped Robots*, pages 185–199. Springer International Publishing, Cham, 2018.
- [37] M. A. Hoepflinger, M. Hutter, C. Gehring, M. Bloesch, and R. Siegwart. Unsupervised identification and prediction of foothold robustness. In *2013 IEEE International Conference on Robotics and Automation*, pages 3293–3298, 2013.
- [38] Stylianos Piperakis, Stavros Timotheatos, and Panos Trahanias. Unsupervised Gait Phase Estimation for Humanoid Robot Walking. In *International Conference on Robotics and Automation (ICRA)*, pages 270–276, 2019.
- [39] M. Camurri, M. Fallon, S. Bazeille, A. Radulescu, V. Barasuol, D. G. Caldwell, and C. Semini. Probabilistic contact estimation and impact detection for state estimation of quadruped robots. *IEEE Robotics and Automation Letters*, 2(2):1023–1030, April 2017.
- [40] Tzu-Yuan Lin, Ray Zhang, Justin Yu, and Maani Ghaffari. Legged robot state estimation using invariant kalman filtering and learned contact events. In *5th Annual Conference on Robot Learning*, 2021.

- [41] V. Ortenzi, H. Lin, M. Azad, R. Stolkin, J. A. Kuo, and M. Mistry. Kinematics-based estimation of contact constraints using only proprioception. In *2016 IEEE-RAS 16th International Conference on Humanoid Robots (Humanoids)*, pages 1304–1311, Nov 2016.
- [42] Michael Maravgakis and Stylianos Piperakis. LCD: Legged Contact Detection. <https://github.com/MichaelMarav/lcd>.
- [43] Jemin Hwangbo, Joonho Lee, and Marco Hutter. Per-contact iteration method for solving contact dynamics. *IEEE Robotics and Automation Letters*, 3(2):895–902, 2018.
- [44] Nathan Koenig and Andrew Howard. Design and use paradigms for gazebo, an open-source multi-robot simulator. In *2004 IEEE/RSJ International Conference on Intelligent Robots and Systems (IROS)*, volume 3, pages 2149–2154. IEEE, 2004.
- [45] Stylianos Piperakis. lipm\_motion: Linear inverted pendulum based motion planning. [https://github.com/mrsp/lipm\\_motion](https://github.com/mrsp/lipm_motion).
- [46] S. Piperakis. lipm\_control: Linear inverted pendulum based control. [https://github.com/mrsp/lipm\\_control](https://github.com/mrsp/lipm_control).
- [47] S. Piperakis, E. Orfanoudakis, and M. Lagoudakis. Predictive Control for Dynamic Locomotion of Real Humanoid Robots. In *IEEE/RSJ Intl. Conf. Intel. Robots and Systems*, pages 4036–4043, 2014.
- [48] Stéphane Caron, Abderrahmane Kheddar, and Olivier Tempier. Stair Climbing Stabilization of the HRP-4 Humanoid Robot using Whole-body Admittance Control. In *International Conference on Robotics and Automation (ICRA)*, pages 277–283, 2019.
- [49] Stylianos Piperakis. whole\_body\_ik: Whole-body Hierarchical Inverse Kinematics. [https://github.com/mrsp/whole\\_body\\_ik](https://github.com/mrsp/whole_body_ik).
- [50] Alessio Rocchi, Enrico Mingo Hoffman, Darwin G. Caldwell, and Nikos G. Tsagarakis. OpenSoT: A whole-body control library for the compliant humanoid robot COMAN. In *IEEE International Conference on Robotics and Automation (ICRA)*, pages 6248–6253, 2015.
- [51] Michael Maravgakis. PCE: Probabilistic Contact Estimation. <https://github.com/MichaelMarav/ProbabilisticContactEstimation>.
- [52] Robert Mahony, Tarek Hamel, and Jean-Michel Pflimlin. Nonlinear complementary filters on the special orthogonal group. *IEEE Transactions on Automatic Control*, 53(5):1203–1218, 2008.
- [53] JooSeuk Kim and Clayton D Scott. Robust kernel density estimation. *The Journal of Machine Learning Research*, 13(1):2529–2565, 2012.